Running Head: Stratigraphic Evolution Of Onlap

Title: The Stratigraphic Evolution of Onlap in Siliciclastic Deep-Water Systems: Autogenic Modulation of Allogenic Signals

Authors: EUAN L. SOUTTER[1*], IAN A. KANE[1], ARNE FUHRMANN[1], ZOË A. CUMBERPATCH[1] and MADS HUUSE[1]

Institutions:

[1]Department of Earth and Environmental Sciences, University of Manchester, Oxford Road, Manchester M13 9PL, UK

Email: euan.soutter@manchester.ac.uk

Keywords: Deep-water, confined basin, onlap, autogenic, Grès d'Annot

ABSTRACT

Seafloor topography affects the sediment gravity flows that interact with it. Understanding this interaction is critical for accurate predictions of sediment distribution, paleogeography, and structural reconstructions of deep-water basins. The effects of seafloor topography can be seen from the bed scale, through facies transitions toward intra-basinal slopes, to the basin scale, where onlap patterns reveal the spatial evolution of deep-water systems. Basin-margin onlap patterns are typically attributed to allogenic factors, such as sediment supply signals or subsidence rates, with few studies emphasizing the importance of predictable spatio-temporal autogenic flow evolution. This study aims to assess the autogenic controls on onlap by documenting onlap styles in the confined Eocene-to-Oligocene deep-marine Annot Basin of SE France. Measured sections, coupled with architectural observations, mapping, and paleogeographical interpretations, are used to categorize onlap styles and place them within a generic stratigraphic model. These observations are compared with a simple numerical model. The integrated stratigraphic model predicts that during progradation of a deep-water system into a confined basin successive onlap terminations will be partially controlled by the effect of increasing flow concentration. Initially thin-bedded low-density turbidites of the distal lobe fringe are deposited and drape basinal topography. As the system progrades these beds become overlain by hybrid beds and other deposits of higher-concentration flows developed in the proximal lobe fringe. This transition is therefore marked by intra-formational onlap against the underlying and lower-concentration lobe fringe that drapes the topography. Continued progradation results in deposition of lower-concentration deposits in the lobe off-axis, resulting in either further intra-formational onlap against the lobe fringe or onlap directly against the hemipelagic basin margin. Basinal relief is gradually reduced as axial and higher-volume flows become more prevalent during progradation, causing the basin to become a bypass zone for sediment routed down-dip. This study presents an autogenic mechanism for generating complex onlap trends without the need to invoke allogenic processes. This has implications for sequence-stratigraphic interpretations, basin subsidence history, and forward modeling of confined deep-water basins.

INTRODUCTION

Deep-water lobes are amongst the largest sedimentary bodies on Earth and comprise terrigenous sediment shed from the adjacent continental shelf and slope (e.g., Piper et al., 1999; Talling et al., 2007; Prélat et al., 2010; Clare et al., 2014). They offer a record of Earth's climate and sediment transport history, form valuable hydrocarbon reservoirs, aquifers, and are sites of mineral accumulation (e.g., Weimer and Link, 1991; Hodgson, 2009; Sømme et al., 2011; Bell et al., 2018a). Sediment-gravity-flow evolution across unconfined deep-water settings results in a fairly uniform radial spreading and deceleration of flows, and development of elongate to lobate sedimentary bodies with predictable facies transitions (e.g., Baas, 2004; Hodgson et al., 2009; Spychala et al., 2017).

Sediment gravity flows encountering seafloor topography in confined-basin settings form a range of onlap geometries that are often associated with complicated sedimentary facies (Fig. 1) (e.g., Kneller, 1991; Haughton, 1994; Wynn et al. 2000; McCaffrey and Kneller, 2001; Smith, 2004a; Smith 2004b; Amy et al., 2004; Gervais et al. 2004; Lomas and Joseph, 2004; Smith and Joseph, 2004; Puigdefàbregas et al., 2004; Gardiner, 2006; Mayall et al. 2010; Tinterri et al. 2016; Hansen et al. 2019). The effect of seafloor topography on sediment gravity flows, their deposits, and onlap styles has been studied through outcrop data (e.g., Kneller et al. 1991; Sinclair, 1994; Bakke et al., 2013), subsurface data (e.g., Prather et al., 1998; 2012; Covault and Romans, 2009; Bakke et al., 2013), and numerical models (e.g., Smith, 2004b; Kubo, 2004; Gardiner, 2006; Sylvester et al., 2015) and physical models (e.g., Kneller, 1995; Kneller and McCaffrey; 1995; Amy et al., 2004; Brunt et al., 2004; Kubo, 2004). Seafloor topography is generated by a variety of geological processes, such as: pre-depositional tectonic deformation (e.g., Jackson et al. 2008; Kilhams et al. 2012), syn-depositional tectonic deformation (e.g., Wilson et al., 1992; Haughton, 2000; Grecula et al., 2003; Hodgson and Haughton, 2004; Tomasso and Sinclair, 2004; Kane et al. 2010; Salles et al., 2014), mass transport deposit relief (e.g. Armitage et al., 2009; Ortiz-Karpf et al., 2015; 2016; Kneller et al., 2016; Soutter et al., 2018) and salt diapirism (e.g., Hodgson et al., 1992; Kane et al. 2012; Prather et al. 2012; Oluboyo et al. 2014; Doughty-Jones et al., 2017). Improved prediction of the distribution of sediment gravity flow deposits around seafloor topography is therefore critical for both paleogeographic reconstructions (e.g., Pinter et al., 2017) and stratigraphic hydrocarbon or CO_2 trap risking (e.g., McCaffrey and Kneller, 2001).

The onlap geometry (3D shape of an event bed or sequence of related event beds at pinch-out) and facies (internal sedimentary characteristics of an event bed at pinch-out) (Fig. 1A), herein termed onlap termination, are controlled by: 1) flow magnitude, duration, velocity, thickness, concentration, and sediment composition; 2) the gradient and incidence angle of the counter-slope; and 3) seafloor composition and induration. Typically, high-concentration flows and steep counter-slopes cause abrupt terminations, whereas low-concentration flows and shallow counter-slopes cause draped terminations (Fig. 1) (Smith and Joseph, 2004; Bakke et al. 2013). Flows with a high mud content may also be more prone to varying degrees of rheological transformation approaching counter-slopes, resulting in complicated facies distributions at confining basin margins (Fig. 1) (Barker et al., 2008; Patacci et al., 2014; Southern et al., 2015).

Recent field-based studies on the spatial and temporal evolution of unconfined submarine lobes have used the longitudinal evolution of flows and their associated facies to establish criteria for differentiating lobe sub-environments at the bed scale (e.g., Prélat et al. 2009; Grundvag et al. 2014; Spychala et al. 2017). The applicability of these facies associations to confined lobes and the complex system-scale stacking patterns that they may produce is only recently being investigated (e.g., Marini et al. 2015; Spychala et al. 2015, 2017; Bell et al. 2018b; Fonnesu et al. 2018; Liu et al. 2018). Previous flow-dependant onlap models mainly focussed on end-member geometries (e.g., McCaffrey and Kneller, 2001; Smith, 2004b; Smith and Joseph, 2004). As yet there is no generic model to account for how the wide variety of deposits resulting from the longitudinal evolution of sediment gravity flows will manifest themselves at onlap surfaces through the fill of a confined basin.

This study uses the well-constrained Cenozoic Annot Basin of SE France to integrate bed-scale and basin-scale onlap observations into a generically applicable depositional model. The aims of this study are to: i) reappraise the Annot Basin stratigraphy with respect to specific deep-water sub-environments, with particular emphasis on the poorly studied eastern exposures of the basin, ii) document lateral facies changes within beds approaching the basin margin and relate these facies changes to longitudinal flow evolution, iii) assess how the longitudinal evolution of confined flows impacts onlap geometry and

99 stacking patterns, and iv) integrate these observations into a generic model for the evolution of onlap in
100 deep-water basins.

101 ## THE ANNOT BASIN

102 ### *Basin Structure*

103 The 160-km-long and 80-km-wide (Clark and Stanbrook, 2001) Cenozoic foreland basin of the
104 western Alps formed due to SW-directed collision of the Adria and European plates, and subsequent
105 loading of the European plate by the Alpine orogenic wedge (Figs. 2, 3) (e.g., Ford et al., 1999). This
106 orogenic deformation is represented in the foreland-basin stratigraphy by a progressive younging to the
107 southwest (e.g. Ford et al., 1999; Du Fornel et al. 2004). Sediment deposition in the basin was affected by
108 complicated basinal topography (e.g., Joseph and Lomas, 2004), which formed due to Late Cretaceous
109 northward-directed Pyrenean compression that was subsequently overprinted by Cenozoic SW-directed
110 Alpine compression (Fig. 3) (e.g., Apps et al., 2004). This resulted in NW-SE-oriented synclinal sub-
111 basins with E-W anticlinal sills. The synclines are interpreted as the surface expression of underlying
112 Alpine thrust-fault-propagation folds (Fig. 3) (e.g., Elliott et al. 1985; Apps, 1987; Ravenne et al. 1987).

113 The Annot sub-basin, herein termed the Annot Basin, is one of the exhumed synclinal Cenozoic
114 depocenters in the Alpine foreland basin, representing the proximal end of the deep-marine Annot-
115 Grand Coyer-Chalufy chain of sub-basins (Figs. 2, 3) (see Joseph and Lomas, 2004, for review). The
116 Annot Basin is bounded to the south by the SW-NE Rouaine Fault Zone, which acted as an entry point
117 for sediment gravity flows into the basin (e.g., Salles et al. 2014) (Figs. 2, 3). The SW-NE Braux normal
118 fault is related to this fault zone and created local bathymetric relief during the Late Eocene (e.g.,
119 Tomasso and Sinclair, 2004) (Figs 3, 4). The western and eastern margins of the basin are defined by
120 fault-propagation anticlines created by Mesozoic blind thrusts (Figs. 3, 4) (e.g., Apps, 1987). The eastern
121 margin is formed by the Melina anticline, or "kink zone" (Apps, 1987), and the western margin by the
122 Puy du Rent anticline (Fig. 3; 4B). These anticlines were developing during deposition of the Annot
123 turbidites, causing syn-depositional rotation of the basin depocenter towards the west (Fig. 3) (e.g., Salles
124 et al., 2014).

E-W-oriented Pyreneo-Provençale structures also affect the Annot Basin structure, with the northern extent of the basin formed by the Aurent anticline (Fig. 3). This structure forms a gently southward-dipping terminal slope (e.g., McCaffrey and Kneller, 2004). More minor basin-floor relief may have been formed by the E-W Fugeret anticline, which lies between the Rouiane fault zone and the Aurent anticline (Fig. 3) (Salles et al., 2014). These E-W-oriented structures show little evidence of major syn-depositional movement due to compressional deformation being dominantly driven by the SW-directed Alpine orogeny during the Eocene and Oligocene.

Stratigraphic Evolution

The Annot Basin has the same transgressive Cenozoic foreland-basin stratigraphy as is seen across the western Alps (Figs. 2, 3) (e.g., Sinclair, 1997), with Oligocene shallow-marine limestones of the Calcaires Nummulitique overlain by deep-marine marls of the Marnes Bleues. The Marnes Bleues records the deepening of the basin, with foraminifera suggesting water depths of ~ 100 m at the base of the succession, to ~ 800 m by the end of deposition (Mougin, 1978). Supply of siliciclastic sediment began abruptly in the Late Eocene (35.2 Ma) as the Corsica-Sardinia massifs were uplifted via subduction-related back-thrusting towards to the south (Fig. 2) (e.g., Stanley and Mutti, 1968; Apps, 1987). This resulted in a depositional shift from the marls of the underlying Marnes Bleues, into south-to-north dispersing clastic sediment gravity flows of the Grès d'Annot. An upwards coarsening trend in the Grès d'Annot suggests progradation of the clastic system, most-likely related to fan-delta advance (Fig. 3) (e.g., Puigdefàbregas et al., 2004).

During early clastic deposition the Annot Basin was located on the western side of a distal submarine fan extending over the foreland basin, with flows entering the basin from syncline-bounded fan deltas to the south (Fig. 2) (e.g., Stanley, 1980; Sinclair, 2000; Joseph and Lomas, 2004) and being dispersed northwards through relay ramps in the Rouaine Fault Zone (Fig. 3) (Joseph and Lomas, 2004; Salles et al., 2014). This early deposition is represented in the Annot Basin by low-density turbidites, often referred to as the Marnes Brunes Inferiérures (e.g., Stanbrook and Clark, 2004), which form the distal equivalent of the Grès d'Annot. The lowermost Grès d'Annot member, termed Le Ray (Puigdefàbregas, 2004) or the A Member (Du Fornel et al., 2004), onlaps both the underlying Marnes Brunes and Marnes

Bleues slope (Fig. 3). Early flows were confined by the Braux Fault to the west, a combination of the Braux Fault and the Fugeret anticline to the north, and the Melina anticline to the northeast (Salles et al., 2014). The sediment entry point shifted throughout deposition of the Grès d'Annot, with a more easterly Late Eocene entry point suggested for these early flows, as evidenced by an up-stratigraphy rotation of paleocurrents from NE- to NW-directed (McCaffrey and Kneller, 2004; Salles et al., 2014). Alternatively, this may be an apparent repositioning of the sediment entry point as the basin depocenter itself migrated gradually westward due to Alpine compression (Salles et al., 2011; 2014). This deformation is believed to have been continuous throughout the fill of the basin; however, the apparent rate of deformation is suppressed in the Grès d'Annot due to the higher depositional rates associated with gravity-flow deposition (Apps et al. 2004). The remaining Grès d'Annot members were confined by the major Melina (east), Puy du Rent (west) and Aurent anticlines (north) as the topography of the Braux Fault and Fugeret Anticline was healed relatively early in the Oligocene (Fig. 3) (Salles et al., 2014).

The basin gradually filled throughout the early Oligocene, with contemporaneous deposition occurring in the parallel Grand Coyer sub-basin to the northeast (Salles et al., 2014). Once the basin was largely filled, the Aurent Anticline ceased to terminally confine flows, and flows bypassed the Annot Basin into the Grand Coyer and Chalufy sub-basins (Fig. 2) (e.g., Apps, 2004; Salles et al., 2014). Few channel fills are seen within the Grès d'Annot succession, and the depositional architecture is interpreted as being predominantly sheet-like (Apps, 1987).

DATA AND METHODS

The dataset comprises 50 (581 m cumulatively) sedimentary logs collected along sections predominantly oriented oblique to depositional-dip along the eastern margin of the Annot Basin (Figs. 3, 4A, 5). Logs were collected at 1:10 scale, and individual beds were walked out at outcrop (Figs. 6, 7). Higher resolution 1:2 scale logs were collected from some beds approaching onlap. Logs within thin-bedded facies were collected at a 1:5 scale to allow accurate representation of their thicknesses and structures. Samples of individual facies and individual beds were collected in order to quantitatively constrain lateral grain-size and matrix changes. 104 3D paleocurrent measurements were collected (Fig. 5), with 2D paleocurrent measurements qualitatively noted.

Margin Correlation

Sedimentological contacts between the discrete members of the Grès d'Annot from the geological maps of Puigdefàbregas et al. (2004), Du Fornel et al. (2004), and Salles et al. (2014) were ground-truthed and compared to observations made by this study (Fig. 3). The observations of stratigraphic contacts made during this study most closely agree with those made by Puigdefàbregas et al. (2004); therefore their geological map was used for placement of sedimentary logs within members and for the intra-member correlation of sedimentary logs (Figs. 5, 6). This allows facies transitions across the basin to be assessed both spatially and temporally. Where member boundaries are unclear due to the resolution of the geological map the top of individual members is defined by either abrupt facies changes, commonly an abrupt coarsening and thickening of event beds, or lateral relationships and correlations (Fig. 5). An attempt has been made to reconcile the nomenclature used by Puigdefàbregas et al. (2004) and Salles et al. (2014) to enable comparisons to be made between the two (Fig. 3).

Detailed correlations of the Le Ray member are based on the identification of key surfaces, such as onlap surfaces, and walking out of individual beds (Fig. 6). Where beds could not be walked out, units were correlated based on the methodology of Prélat et al. (2009) for the identification of the hierarchical elements that builds lobes, e.g., beds, lobe elements, and lobes.

FACIES ASSOCIATIONS

Facies associations (FA) have been interpreted based on the dominant lithofacies (LF) and depositional features of a given succession (Table 1). The dominant lithofacies has been described and interpreted within each facies association in order to justify their placement in that sub-environment. The lobe sub-environments of Spychala et al. (2017) are used because they best fit the observations made in this study (Figs. 8, 9). The onlap geometry of each lithofacies, and therefore the inferred onlap geometry of the facies association in which that lithofacies dominantly occurs, is summarized in Table 1. Facies associations are presented in the following section from proximal to distal positions on the lobe, in descending stratigraphic order and, broadly, in descending order of thickness.

FA 1 Lobe-axis

Observations.--- Facies association 1 is composed dominantly of one lithofacies: thick-bedded (0.5 - 2 m) sandstones (LF 1A) (Figs. 10A, B, E), with thin-bedded (0.01 m - 0.5 m) sandstones (LF 1B) and medium-bedded sandstones (0.1 - 0.8 m) (LF 3) commonly associated. LF 1B is composed of medium- to cobble-grade (most typically coarse-grained), poorly sorted, massive sandstones (Fig. 10B) and is less prevalent than LF 1A. Individual beds have erosional bases, often with groove, flute, and tool marks, and irregular tops. Beds are often lenticular, thickening and thinning from < 10 cm before pinching out over tens of meters. The beds often occur within successions of medium-bedded sandstones (LF 2) below packages of LF 1.

The thick-bedded LF 1A sandstones are medium-grained to granular sandstones with bed bases that are flat (at exposure scale) or erosional (Figs. 7, 11B). Flat bases are most prominent when overlying mudstones, while erosional bases are most commonly expressed as amalgamation surfaces (Fig. 9B, C, D). Both bedding-parallel and erosional bases are associated with decimeters of deformation in the underlying beds. This deformation obscures the primary depositional characteristics of the underlying beds, making interpretation of the deformed beds difficult. Bed bases with steeper dips than the bed top are observed at pinch-out of these beds (Fig. 11B), with bed bases steepening towards the pinch-out. Amalgamation surfaces are identified by mudstone-clast-rich rugose horizons, abrupt grain-size breaks, and truncated trace-fossil burrows. Bed tops are flat and exhibit little depositional relief. Beds are typically

structureless, with rarely preserved faint parallel lamination and tractional structures, and ungraded, though some beds show weak normal grading (Figs. 7, 9B, C, D).

Interpretations.--- The presence of erosional bed bases with tool marks and grooves indicates that LF 1A beds were deposited by high-concentration flows that initially carried large clasts and other detritus at the base of the flow. Superimposed flute marks, normal grading, and tractional structures are indicative of evolution to a less concentrated, more turbulent flow. The rarity of tractional structures and commonly massive and poorly sorted beds, however, indicates that these beds were deposited rapidly (*sensu* Lowe, 1982). This is most likely due to a reduction in flow capacity (*sensu* Hiscott, 1994), preventing the formation of grading and the preservation of bedforms. These turbidites are therefore interpreted as high-density turbidites (*sensu* Lowe, 1982). The presence of deformation structures beneath these flows has been attributed to high shear stresses acting on the seabed (e.g. Clark and Stanbrook, 2001; Puigdefàbregas et al. 2004). These laterally extensive (up to 1 km where outcrop allows) high-density turbidites, which are commonly amalgamated, are interpreted to be analogous to lobe axis deposits observed elsewhere (e.g., Prélat et al. 2009).

The coarse grain size and thin-bedded nature of LF 1B suggests that these beds were deposited as a coarse-grained lag in a bypass-dominated part of the system. The lenticular geometry suggests that either i) flow energy, and therefore bypass potential, was not homogeneous laterally within the flow or ii) erosion by later flows or waxing of the flow (Kane et al., 2009), scoured the bed top (Fig. 10B). Because this lithofacies is confined stratigraphically to sequences underlying thick-bedded and amalgamated sandstones of similar grain sizes, they are inferred to be laterally related. These lags are interpreted to represent a mostly bypassing equivalent of the thick-bedded sandstones in the lobe axis.

FA 2: Lobe off-axis

Observations.--- Facies association 2 is composed primarily of normally graded medium-bedded (0.1 - 0.8 m) fine- to medium-grained sandstones (LF 2) with flat to slightly erosional bed bases and flat bed tops (Figs 7, 10A, 12). Flutes and grooves are often seen at bed bases. Ripples at bed tops commonly show opposing paleoflow directions to those measured from flutes and grooves on individual event beds (Fig. 5). Beds pinch out abruptly towards the basin margin, and often can be traced away from the onlap

surface to a parent thick-bedded sandstone (Fig. 7). In the uppermost stratigraphy of the basin, LF 2 commonly has highly irregular bed tops with abundant tractional structures, such as climbing ripples and convolute lamination (Figs. 10E, 12). These beds are termed LF 2B.

Interpretations.--- The presence of flutes, normal grading, and tractional structures indicate that the LF 2 beds were deposited by waning, turbulent flows which were able to rework the aggrading deposit (Bouma, 1962). This suggests that these flows were more dilute than the parent flows of the thick-bedded sandstones (LF 1). These medium-bedded sandstones are therefore interpreted as medium-density turbidites and are differentiated from low-density turbidites by bed thicknesses being greater than 10 cm and a coarser grain size. These medium-density turbidites also have a thicker massive interval at their base compared to low-density turbidites. Opposing paleocurrent directions within event beds is characteristic of flows encountering topography (e.g., Kneller et al., 1991), indicating that many of these beds were deposited close to a basin margin. Coarser, denser parts of the flow may be more strongly influenced by topography than the upper more dilute part of the same flow (Bakke et al., 2013).

The finer, better sorted and thinner-bedded nature of this lithofacies compared to thick-bedded sandstones indicates that these beds were deposited beyond the axis of the lobe (off-axis) (Prélat et al. 2009; Bell et al., 2018a) (Fig. 8). LF 2B is interpreted as representing flows that were deposited close to the basin margin or possibly within slump scars on the basin margin. Bypassing flows deflected by the margin or trapped in scars caused complicated oscillatory-flow patterns to develop which deformed the aggrading deposits (Pickering and Hiscott, 1985; Tinterri et al. 2016; Cunha et al. 2017). An example of this can be seen at Tête de Ruch, where this facies dominates a ~ 10 m thick scar fill (Puigdefàbregas et al. 2004) and is overlain by thin beds showing simple uniformly directed ripples and plane-parallel lamination (Figs. 5, 11C). These thin beds were deposited over the scar fill where flows were relatively unconfined, allowing more uniform and waning flow deposition to dominate.

FA 3: Proximal fringe

Observations.--- Facies association 3 is dominated by medium- to thick- bedded (0.1 m - 1.2 m) bipartite or tripartite event beds (LF 3) (Figs. 9, 11C, D, G). These beds are composed of a lower division of medium- to thick-bedded sandstone (LF 1 and LF 2) with an irregular top which is loaded and/or

eroded into by an overlying argillaceous sandstone (Fig. 10D). The middle division is an argillaceous sandstone, poorly sorted and often deformed, which appears as a sheared fabric (Fig. 10D). The argillaceous sandstone can either contain clasts of the underlying sandstone or be clast-poor. Organic matter (< 70 cm in length) may be present in this bed, with organic-rich sandstones typically thicker than the more argillaceous sandstones. Elongate organic matter is usually aligned with its long axis approximately parallel to paleoflow recorded on the bed base (Fig. 10C).

Argillaceous sandstones, which are rich in cleaner sandstone clasts, commonly occur where the lower, cleaner sandstone is coarser-grained; thus most sandstone clasts seen tend be coarse-grained than the argillaceous matrix. This deposit can show variable sand-to-mud ratios. Higher sand contents within this middle division are associated with increased prevalence of lamination, with centimeter-scale layering (mud-concentrated laminae) sometimes evident, and higher mud contents associated with more sheared and poorly sorted deposits. Both of these divisions may contain coarse-sand to granule-size quartz grains supported within the matrix.

Overlying this argillaceous sandstone, medium-bedded, often muddy sandstone may occur, although it is sometimes difficult to assess whether this sandstone is part of the underlying event bed or represents a separate event bed (Fig. 10D). This sandstone has an irregular base and can show loading and foundering into the underlying argillaceous sandstone (Fig. 10D). The bed top is typically flat or mounded. Approaching basin margins these beds can be seen to transition laterally from thick-bedded sandstones (Fig. 13A, B).

The middle division of the bed may pinch out between the underlying and overlying sandstones, which then amalgamate at the onlap surface (Fig. 13C), forming a complicated and often muddy pinch-out (Fig. 14). Stratigraphically this lithofacies dominantly occurs following the thin-bed-dominated sequence and underlying the medium- to thick-bedded sandstones (Fig. 9).

Interpretations.--- The basal and upper sandstones within these bipartite or tripartite event beds are interpreted as either high-density or medium-density turbidites. The massive, poorly sorted, and mud-rich nature of the division encased by these turbidites is interpreted as being caused by en-masse deposition of a laminar and cohesive flow (e.g., Middleton and Hampton, 1973; Mulder and Alexander,

303 2001). This bed division is therefore interpreted as a debrite. The irregular contact seen between these
304 divisions has been attributed to complex short-wavelength soft-sediment deformation and erosion (e.g.,
305 Fonnesu et al. 2015). Where the overlying turbidite is relatively thick it is difficult to differentiate between
306 a debritic or deformed (see LF 1 basal deformation) origin for the middle division, particularly when the
307 overlying turbidite has foundered into the underlying division (e.g., Fonnesu et al. 2015). Where the
308 middle sandstone division is slightly cleaner, with lamination and/or layering, the sandstone is interpreted
309 as having been deposited by flows transitional between laminar and turbulent and therefore termed a
310 transitional-flow deposit (Baas et al., 2011; Kane and Pontén, 2012). These tripartite event beds therefore
311 contain deposits of both turbulent and laminar flow regimes and are subsequently interpreted as hybrid
312 beds (*sensu* Haughton et al., 2003; 2009).

313 It is suggested that the more organic-rich linked debrites, with decimeter clasts of terrestrial
314 debris, are derived from flows which originated from events in the hinterland that carried significant
315 amounts of terrestrial debris into the marine environment (see also Hodgson, 2009). These beds are
316 therefore deposits from particularly high-magnitude flows; this may explain their greater average thickness
317 compared with the more argillaceous hybrid-beds. It is also possible that the organic material was staged
318 for significant periods of time on the shelf, making terrestrial debris a poor indicator of flow magnitude.
319 The close association of terrestrial debris and coarse grain sizes in these relatively distal environments,
320 however, indicates that these beds were the result of high-magnitude or "outsize" flows that were capable
321 of significant substrate erosion (Fonnesu et al. 2018). Incorporation and disaggregation of this eroded
322 substrate will have primed these flows for rheological transformation (Kane et al. 2017; Fonnesu et al.
323 2018). LF 1 can be seen to transform into these hybrid beds over tens of meters approaching the slope,
324 further indicating that these beds were highly erosive and prone to rheological transformation, even in
325 proximal positions, due to forced deceleration against the basin margin (e.g., Patacci et al. 2014). The
326 presence of large amounts of erodible and muddy draping substrate on the basin margin will aid in short-
327 length-scale flow transformation in these high-magnitude flows (Fig. 14) (e.g., Fonnesu et al. 2018).

328 It is possible that the debritic division of these beds represents high-concentration turbidity
329 currents hitting the counter-slope, causing intra-basinal slope instability and failure. The turbidity current

will then have aggraded around this failure, represented depositionally by a sandwiched debrite (e.g., McCaffrey and Kneller, 2001). It is difficult to differentiate between a flow-transformation or slope-failure origin for the co-genetic debrite at outcrop; however, the presence of large organic clasts within an identified debritic division may favor a flow-transformation origin.

Because these beds dominantly underlie the thicker-bedded and more sandy turbidites of FA 1 and 2, they are interpreted as being depositionally adjacent (*sensu* Walther, 1894) (Figs. 8, 9). An abundance of hybrid beds indicates a more distal lobe sub-environment compared with the axis and off-axis deposits of FA 1 and FA 2 (e.g., Hodgson, 2009; Jackson et al. 2009; Kane et al., 2017; Fonnesu et al. 2018). This sub-environment is termed the lobe fringe. FA 3 is therefore interpreted as being analogous to lobe-fringe deposition seen in unconfined systems (e.g., Spychala et al. 2017). The lobe fringe can be further subdivided into a lateral and frontal fringe, with the lateral fringe having a lower proportion of hybrid beds compared to the frontal fringe (Spychala et al. 2017). In confined settings this definition is complicated because flow deceleration against lateral slopes cause flow transformations and subsequent enrichment of hybrid beds in the lateral fringe (Figs. 8, 15, 16, 17). This relationship is also evident in the Late Cretaceous Britannia Sandstones of the North Sea, where flows underwent rheological transformation against a lateral slope (Lowe and Guy, 2000; Barker et al. 2008). This study thus uses the general term proximal fringe because the frontal and lateral fringe are expected to be similar due to the counter-slope causing a prevalence of hybrid beds in both settings (Figs. 8, 14, 17).

It should also be noted that particularly erosive flows in the lobe axis and off-axis also generate hybrid beds at the onlap surface (e.g., Patacci et al. 2014; Fonnesu et al. 2018). This can make lobe-sub-environment interpretation challenging when adjacent to a steep basin margin because much of the succession may be margin-affected over short length scales (tens of metres) (Fig. 14) and therefore not represent their primary lobe-scale paleogeographic position (e.g., Southern et al. 2015). This is enhanced in tectonically active basins where flow types can be highly variable (e.g., Mutti et al. 2009). Facies back-stripping may therefore need to be attempted to assess the lobe-scale sub-environment (Fig. 16). These short-length-scale margin effects and attempts at back-stripping are summarized in Figure 16 and 17.

FA 4: Distal fringe

Observations.--- Facies association 4 is dominated by thin-bedded (0.01 – 0.1 m) siltstones to fine-grained sandstones (LF 4) that form laterally continuous event beds (Figs. 7, 11A, 14). Parallel and convolute lamination is common (Fig. 10F). Beds are normally graded, with ripples common on bed tops (Fig. 10F). Ripples may show multiple and opposing paleocurrent directions within single beds. Beds tend to pinch out over tens to hundreds of meters towards the basin margin (Fig. 15), with amalgamation of event beds sometimes observed towards the onlap surface, causing local bed thickness increases in a regional thinning trend. Slumping and folding of beds (LF 5) is evident in this FA, particularly immediately underlying the abrupt transition to dominantly medium- and thick-bedded sandstone sequences (Fig. 10G). Fold-axis measurements indicate that deformation was both oblique and perpendicular to paleo-slopes. Stratigraphically, these beds immediately overlie the Marnes Bleues, forming a distinct sequence that significantly drapes the Marnes Bleues slope (11A). This lithofacies becomes less common up stratigraphy (Fig. 9).

Interpretations.--- The fine grain-size, abundance of tractional structures, and dominance of thin beds within LF 4 indicates deposition from dilute, low-density turbidity currents (*sensu* Lowe, 1982). The narrow grain-size range (dominantly silt) of these slope-draping beds is numerically predicted because of the quadratic decrease in settling velocity of silt and mud and the consequent increase in likelihood of flow inflation far above the initial flow depth in silt- and mud-rich flows (Dorrell et al. 2019). Because these beds are able to drape the existing relief they are suggested to have healed much of the initial relief present on the Marnes Bleues slopes (Figs. 7, 11A). Slumping in these successions (LF 5) is interpreted to represent slope failure on the steep basin margins (Fig. 10G). Progressive deformation and seismicity along the Alpine thrust front is suggested as the primary reason for slope failure (Fig. 2). Failure scars may contribute to some of the heterogeneity seen within the overlying medium- and thick-bedded sandstones by creating a rugose topography high on the slope (Fig. 11C).

The lateral continuity, fine grain-size and thin-bedded character of the thin beds is consistent with both levee deposition and lobe-fringe deposition. Because of the few long-lived channels identified and the low stratigraphic position of these beds in a prograding lobe (Fig. 9), they are not interpreted to be levee deposits, but are instead attributed to the distal fringe of a submarine lobe on the basin floor (e.g.,

Boulesteix et al. 2019a, b) (Fig. 8), which caused termination of Marnes Bleues carbonate deposition. This is supported by the published paleogeographic position of the lowermost Grès d'Annot (Fig. 2) (Apps et al., 2004; Joseph and Lomas, 2004; Salles et al., 2014). The relative lack of hybrid beds in the LF5 sequence also supports a distal lobe fringe interpretation (Figs. 8, 9A, 13) (Spychala et al., 2017).

STACKING PATTERNS

Le Ray

Confined basins have previously been associated with sheet-like deposition, where incoming flows are entirely confined by the basin margins, resulting in tabular stratigraphy with little or no autogenic compensational stacking (e.g., Sinclair and Tomasso, 2002). Numerical studies (Dorrell et al. 2018), subsurface studies (e.g., Beaubouef and Friedmann, 2000), and outcrop studies (e.g., Spychala et al. 2016; Bell et al. 2018b; Liu et al. 2018), however, have shown the stacking-pattern complexity that may arise in basins that display variable degrees of confinement. This study uses data from the lowermost member of the Grès d'Annot, the Le Ray member (Figs 5, 6), to build on these studies. Le Ray (Puigdefàbregas et al., 2004), or member A (Du Fornel et al. 2004), was fully confined by the basin margins during its deposition (Callec, 2004; Salles et al. 2014).

Unit 1.--- This unit comprises a sequence of thin-bedded low-density turbidites (LF 4) overlain abruptly by medium- and thick-bedded high-density turbidites (LF 1 and 2). These thick-bedded sandstones correlate with a thick sequence of thin-bedded turbidites ~ 800 m to the NW adjacent to the Braux Fault footwall (Figs 3, 6). This transition is caused either by flow over-spill across the paleobathymetry of the Braux Fault or draping of the lower-density part of the flow up the Braux Fault topography. Correlation of this unit toward the NE is hindered by lack of exposure; however, it is possible that the distal Unit 1 correlates with some of the early Unit 2B deposition (Fig. 6).

Unit 2.--- Proximal Unit 2 is characterized by a thick 33 m amalgamated sandstone body interpreted as being deposited by high-concentration turbidity currents. Indicators of erosion, such as scours and decimeter-scale mud-clasts, indicate that this was a region of significant bypass (e.g., Stevenson et al. 2015) and is interpreted to represent the lobe axis (FA 1) through Le Ray deposition. Down-dip this unit has been subdivided into Unit 2A and 2B based on facies and stacking. Unit 2B is

411 composed of thin-bedded turbidites that drape the frontal confinement of the early Annot Basin and
412 stack aggradationally (Fig. 11A). This confinement was caused by a combination of the basin closure due
413 to the NW-SE Melina anticline, the E-W Fuguret anticline, and the NE-SW Braux Fault (Fig. 3). Unit 2A
414 represents an abrupt transition into thicker-bedded sandstones that pinch out against the underlying Unit
415 2B. These sandstones can be subdivided into various lobes based on the correlation of intervening
416 packages comprising low-density turbidites (LF 4) overlain by hybrid beds (LF 3), medium-density
417 turbidites (LF 2), and amalgamated high-density turbidites (LF 1), which are interpreted to represent the
418 sequential stacking of distal-fringe (FA 4), proximal-fringe (FA 3), off-axis (FA 2), and axis deposits (FA
419 1). These lobes represent the depositional products of the bypassing flows from the proximal thick
420 sandstone body, forming the lobe axis.

421 The axis of each of these lobes steps farther into the basin, suggesting allogenic progradation
422 through increasing sediment flux from the uplifting Corsica-Sardinia hinterland (e.g., Apps et al. 1987).
423 This pattern is not uniform, however, and a degree of compensational stacking is clearly visible, with the
424 axes of successive lobes (represented by amalgamated high-density turbidites) overlying the fringes of
425 underlying lobes, which represented lows on the seafloor (e.g. Deptuck et al. 2008; Prélat et al. 2009).
426 These stacked lobes could also represent lobe "fingers" that were focussed between the lows of the
427 previous axial deposits (e.g., Groenenberg et al. 2010). In this case the apparent basinward stepping of the
428 Le Ray lobes may be autogenically-driven, as flows are focussed between the lows and build passively into
429 the basin. This explanation may operate in tandem with allogenic progradation, particularly during early
430 deposition, due to the prevalence of these finger-like geometries in the basal stratigraphy of lobe
431 complexes (e.g., Prélat et al. 2009; Groenenberg et al. 2010). These indicators of compensational stacking
432 are at odds with the prevailing suggestion that basins generically described as "confined" can be assumed
433 to have a sheet-like architecture, and fit with the recent work indicating that lobes deposited within basins
434 with varying degrees of confinement are characterized by more complicated stratigraphic relationships
435 (e.g., Marini et al. 2015; Bell et al. 2018b; Liu et al. 2018).

436 The presence of thick and coarse sandstones in distal positions has also been described in
437 subsurface datasets of submarine lobes and lobe elements and has been attributed to flow stripping of the

upper dilute parts of flows over the basin's confining topography, leaving behind the coarser parts of the flow (e.g., Marini et al. 2016; Jobe et al. 2017). This process may also contribute to the preservation of the thick and abruptly terminating sandstones within Unit 2A of the Le Ray member.

Unit 3.--- This unit has been differentiated because it cannot be reliably correlated to another unit. It is possible that Unit 3 represents the distal expression of the upper parts of Unit 2, however the lack of exposure between the proximal and distal parts of the upper Le Ray prevents reliable correlation.

Alternative Interpretations.--- The observed intra-formational onlap against the low-density fringe (Unit 2B) at the Col du Fa locality is likely caused by the inferred proximity of the basin margin. An alternative explanation for this stratigraphic relationship may be the presence of a large erosional feature, such as a scour, at the Col du Fa margin. Such scours are interpreted higher in the basin stratigraphy at Tête du Ruch (e.g., Puigdefàbregas et al. 2004), and show the same intra-formational onlap relationship (Fig. 11C). Decameter-thick scour fills are also suggested to be present in the Grès d'Annot at Peira Cava (Lee et al. 2004). The scour would have created accommodation space to be filled by the incoming flows, resulting in the onlap geometries described by this study. Exposure limits further analysis of this problem, however, a scour interpretation is not believed to affect the underlying principles of this study as the low-density turbidites still drape the scour and are onlapped by the later higher-density turbidites.

Another explanation for the observed intra-formational onlap may be that the low-density fringe (Unit 2B) was tilted (e.g., Salles et al. 2014) and subsequently onlapped by higher-density flows when the basin was relatively static or depositional rates were higher, resulting in the wedge-shaped geometry observed (Apps et al. 2004). Unit 2B may therefore represent the distal extents of early Le Ray (i.e., Unit 1), while the onlapping Unit 2A is either more proximal and late-stage Le Ray or early La Barre (i.e., Unit 3) (Figs. 3, 5). Differential compaction between the basin center and the basin margin may have also acted to enhance the tilting effect (Sinclair, 1994). The inability to walk out individual units between outcrop localities again makes further analysis of this problem difficult. If tectonism or differential compaction is the reason for the observed relationship, then run-up of the low-density turbidites that characterize Unit 2B would have acted to exaggerate the intra-formational onlap that was caused by tilting, and the underlying principles of this study are maintained. Unit 1 would therefore be analogous to the ponded

aprons identified in intra-slope basins of the Gulf of Mexico, while Unit 2 would similar to a perched apron (Prather et al. 2017).

Turbidity-Current Run-Up and Onlap Geometry

Sediment gravity flows are able to deposit high on confining slopes through flow run-up and/or inflation (e.g., Muck and Underwood, 1990; Lamb et al. 2008; Dorrell et al. 2019). The distance a turbidity current runs up topography is termed the run-up height (H) and, in its simplest form (following Straub et al. 2008), can be represented by,

$$H = h + \frac{\rho_c U^2}{(\rho_c - \rho_a) 2g} \quad (1)$$

Where h = flow thickness, U = flow velocity, ρ_c = bulk density of the flow (composed of quartz at 2650 kg m^{-3}), ρ_a = density of the ambient water (seawater at 1020 kg m^{-3}), g = acceleration due to gravity (9.81 m s^{-1}). In order to assign a single value for sediment concentration there is an assumption that there is no density stratification within the flow. A 30-m-deep channel-form at Chambre du Roi (Sinclair, 2000) has been used as the basis for estimating minimum flow height. This is slightly arbitrary but serves the purpose of this thought-experiment. In order to correct for channel-related superelevation, this flow height has been multiplied by 1.3 (see Mohrig and Buttles, 2007), giving a h value of 39 m. This height represents the minimum height of the flow at the lobe apex, disregards compaction, and is assumed constant. It should be noted that due to a lack of flow height proxies preserved at outcrop this value is used purely to demonstrate the underlying principles of the model, i.e., the model does not attempt to fully reconstruct the turbidity currents entering the Annot Basin. The depth-averaged flow velocities used range from 5 m s^{-1} to 0.5 m s^{-1}. The upper limit of 5 m s^{-1} is derived from the maximum flow velocities (4 - 6 m s^{-1}) reached by sand-rich flows in the Monterey Canyon (Symons et al. 2017), while the lower limit of 0.5 m s^{-1} is derived from average measurements of finer-grained flows in the Congo Canyon (Azpiroz-Zabala et al. 2017). The Annot system is sand-rich; therefore the faster Monterey flows are likely the most analogous, at least close to the input. Flow velocity will decrease with decreasing concentration, making the use of a constant velocity problematic. This is suggested to be less important for small and confined basins, such as the Annot Basin, where flows may be prevented from significant velocity decay between

491 the axis and pinch-out. If velocities do decay significantly, then plotting single velocity values through the
492 height of an individual flow will be required; for example, the 5 ms^{-1} and 10% concentration basal part of
493 a hypothetical flow will run-up 9.2 m above the flow height, while its 1 ms^{-1} and 0.1% concentration tail
494 will run-up 32 m above the flow height. This decameter scale difference may explain the ~ 15 m of slope
495 drape at Col du Fa (Figs. 6, 8). This parameter is further complicated by the possible presence of low-
496 velocity dense basal layers within highly-concentrated stratified flows (e.g., Stevenson et al. 2018).
497 Turbulence is suppressed in these basal layers; this reduces velocity and run-up heights, resulting in the
498 increased likelihood of an abrupt pinch-out of the sand-rich basal layer and bypass of the upper and low-
499 concentration parts of the flow. The wedged high-density turbidites identified at onlap by this study (Fig.
500 11B) may be the depositional products of such basal layers.

501 By varying flow concentration in equation (1), a clear trend is developed, with lower sediment
502 concentrations resulting in greater run-up heights (Fig. 18A). In prograding lobe systems turbidity
503 currents with lower sediment concentrations (well below 10%), forming low- or medium-density
504 turbidites, are typically found in the distal or basal stratigraphy and flows with higher sediment
505 concentrations (> 10%), forming high-density turbidites, are typically found in the proximal or upper
506 stratigraphy (e.g., Hodgson et al. 2006, 2009; this study). This therefore suggests that earliest turbulent
507 flows into a receiving basin should have the greatest run-up heights, assuming all of these flows are of
508 similar thickness, with run-up heights decreasing through time as flows become more concentrated (Fig.
509 18A). It should be noted that the effect of increasing concentration through time will be counteracted by
510 increasing velocities, as discussed previously. Suspended-sediment concentrations of > ~ 8% have been
511 shown to suppress the generation of current ripples and cause transformation from turbulent to
512 transitional flow, where flows decelerate sufficiently, forming transitional or hybrid-flow deposits (Baas et
513 al. 2011). This concentration (> ~ 8%) has therefore informed the placement of hybrid beds along the x-
514 axis of the run-up height trend (Fig. 18A), giving hybrid beds a similar run-up potential as high-density
515 turbidites. It should be noted that Baas et al. (2011) emphasize that this value is dependent on flow
516 velocity, grain size, and sediment composition, and that the dimensionless Reynolds number is a much
517 better predictor of flow phase. The results of this analysis fit with facies-dependant thinning rates
518 compiled from 18 outcrop studies by Tő kés and Patacci (2018), with hybrid-beds having 1.3 to 2.8 times

519 higher thinning rates than turbidites. Data collected in this study also support the compiled data of Tő kés
520 and Patacci (2018), with thinner-bedded turbidites having lower thinning rates than thicker-bedded
521 turbidites and consequently draping topography (Figs. 6, 7, 15). Similar thinning trends have been
522 reported from levee sandstones (DeVries and Lindholm. 1994).

523 *Lateral vs. Frontal Onlap*

524 To assess the run-up variation between frontal and lateral onlap the velocity of the modeled flow
525 (at 5% concentration) was varied according to the incidence angle of the flow with the slope. It is
526 assumed that the flow velocity will be at its maximum (5 m s^{-1} in this case) in the principal direction of
527 travel, or an angle of incidence of 90° with respect to the slope, and that the flow velocity will fall to 0 ms^{-1}
528 perpendicular to its axis at an angle of incidence of 0°, i.e., when the flow is running perpendicular to the
529 topography. In reality there will still be some lateral velocity; however, for the purposes of this simple
530 analysis it is assumed that this is negligible. The fastest flows occur at an angle of incidence of 0° or
531 perpendicular to the slope (Fig. 18B). These flows therefore run farther up the counter-slope. Deposits of
532 these flows would pinch out higher up the frontal slope than the lateral slope (Fig. 18B, C). In the 5 ms^{-1}
533 case, for example, the difference in run-up height between the frontal and lateral part of the flow is 17 m.
534 The difference will be increased in lower-density flows and reduced in slower flows.

535 DISCUSSION

536 *Stratigraphic Evolution of Onlap*

537 Based on the similarity between facies transitions and associations seen in this confined basin and
538 those in unconfined or weakly confined submarine lobes (Figs. 8, 9) (e.g., Hodgson, 2009; Spychala et al.,
539 2016, 2017), and the onlap termination styles shown by this study to be produced by the parent flows of
540 these facies (Figs. 16, 17), a predictable stratigraphic evolution of onlap at confined basin margins is
541 proposed (Fig. 19).

542 **Distal Fringe.---**Initially, onlap terminations will be characterized by draping of the slope as
543 low-density turbidites of the lobe fringe are deposited (Figs. 17, 19). This low-density turbidite drape is
544 likely to be composed predominantly of silt or mud, because fine-grained flows are much more capable of
545 flow inflation and deposition high on the slope (Dorrell et al. 2018). It is also suggested that much of the

poorly-exposed hemipelagic sediment in deep-marine basins is composed of millimeter-scale and centimeter-scale event beds (Fig. 10F) (Boulesteix et al. 2019a, b), and consequently represents the distal lobe fringe. Lobe-fringe deposition is therefore likely to be more widespread than previously appreciated (Boulesteix et al. 2019b; Spychala et al. 2019) and results in the healing of substantial amounts of basinal topography, forming a dominantly aggradational sequence of thin beds on the basin margin (Figs. 11A, 17, 19).

Proximal Fringe.---Hybrid beds and low-density turbidites of the proximal lobe fringe are then deposited into the basin as the system progrades (Fig. 19). These hybrid flows are more concentrated and will therefore have lower flow efficiencies when they encounter the slope, so will be unable to deposit as far up the slope as the underlying low-density turbidites of the distal lobe fringe (Figs. 17, 18A). This will cause abrupt intra-formational onlap of these higher-concentration flows against the underlying lobe-fringe deposits (Fig. 19). In the Annot Basin this is represented by proximal-fringe deposits wedging out against the underlying distal-fringe deposits (Figs. 11A, 15). The abruptness and complex 3D geometry of these terminations is enhanced by the combined potential for hybrid-bed development through long-run-out cohesive flow transformation (e.g., Haughton et al. 2009), slope-induced flow transformation (e.g., Barker et al. 2008; Patacci et al. 2014; Bell et al. 2018b), and flow-induced slope failures (e.g., McCaffrey and Kneller, 2001) (Fig. 16). This depositional pattern will be seen in cross sections as a progressive migration of termination points towards the basin center (offlap) (Fig. 19) or a reduction in distance between successive onlapping termination points towards the basin margin. Sylvester et al. (2015) generated similar onlap trends using a geometric approach with subsidence and sediment supply as the variables.

Off-Axis.---As progradation continues, these hybrid-bed-prone proximal-fringe deposits will become overlain by deposits of more proximal flows which have not decelerated to the same degree and hence are more turbulent and of lower concentration, but sand-rich (Figs. 17, 19). The off-axis deposits will be able to drape the slope more effectively than the underlying hybrid beds owing to their lower sediment concentrations (Fig. 19). This will result in progressive termination of their deposits higher up

572 on the slope and either intra-formational onlap against the now thinner veneer of the low-density fringe
573 or onlap directly against the hemipelagic basin margin (Figs. 17, 19, 20, 21).

574 **Axis.---**As higher-concentration flows begin to dominate, intra-formational onlap may occur
575 against the underlying fringe or off-axis deposits that were able to run up the hemipelagic slope (Fig. 19).
576 The highly concentrated basal layers of these flows will be preserved as abruptly onlapping high-density
577 turbidites, with the low-density tail of the flow bypassed down-dip. These axial flows will also be more
578 erosive and able to incorporate mud-rich substrate, resulting in an increasing likelihood of intra-
579 formational onlap through short-length-scale rheological flow transformation and consequent higher
580 thinning rates adjacent to the basin margin (Fig. 14). The scours formed by these erosive events close to
581 onlap will promote further autocyclic modulation of stacking patterns adjacent to the basin margin (e.g.,
582 Eggenhuisen et al. 2011). This relationship will also be exaggerated in coarser-grained systems because
583 higher concentration flows will be less able to deposit farther up the slope, particularly at lateral margins if
584 these high-concentration flows are narrower (Al-Jaidi et al. 2004).

585 A critical point in the basin fill will then be reached when these deposits heal the confining
586 topography sufficiently to allow bypass of the coarser components of flows over the confining slope,
587 forming a stepped, instead of a ponded, basin (Prather et al. 2017). Until this level is reached the finer-
588 grained parts of the flows were stripped, thus increasing the sand proportion in the up-dip basin (Prather
589 et al. 2017). This transition is represented toward the sill of the Annot Basin, where proximal lobe-axis
590 deposits bypass down-dip to the Grand Coyer minibasin (Fig. 2), where this stratigraphic evolution
591 repeats in the next confined depocenter.

592 In the case that the topography is sufficient so as not to be healed by the underlying deposits, the
593 lobe-axis deposits will continue to onlap against the underlying deposits until the accommodation is
594 healed sufficiently to allow the axial deposits to onlap against the hemipelagic basin margin or completely
595 fill the basinal relief and behave as essentially unconfined deposits, resulting in downlapping terminations
596 (Fig. 19). Apparent unconfinement in a vertical section may also occur if allogenic progradation (e.g.,
597 increasing sediment flux) does not keep pace with topographic healing. This will result in the axial

598 sandstones rarely onlapping directly against the constantly retreating basin margin and instead depositing
599 away from the slope and on the basin floor (e.g., Kneller and McCaffrey, 1999).

600 *Applicability and Limitations*

601 **Syn-Depositional Deformation.---**This general stratigraphic evolution applies most readily to
602 static basins with little syn-depositional deformation, where onlap trends are not modified by changes in
603 subsidence or depocenter migration (Figs. 19, 21). The Annot Basin was subject to syn-depositional
604 movement of the depocenter (e.g., Salles et al., 2014); however stratigraphic units of the basin fill show
605 the same conceptual evolution as hypothesized for a static basin (Fig. 6), with the only difference being
606 that the onlap is exaggerated on the tilted eastern exposures because of the increasing slope angle during
607 deposition (Fig. 11A) (Salles et al. 2014). In salt-deformed basins, where syn-depositional subsidence can
608 be rapid, this onlap evolution will be also be exaggerated. The general model for onlap evolution (Fig. 19)
609 may therefore broadly apply to actively deforming basins (Fig. 21). It may be difficult, however, to
610 differentiate between allogenic onlap patterns caused by syn-depositional subsidence or sediment flux
611 (e.g., Sylvester et al., 2015) and those caused by autogenic variations in flow properties (Fig. 21). Care
612 therefore needs to be taken when reconstructing tectonic histories from onlap trends alone, especially in
613 datasets without lithological control.

614 **Onlap Incidence Angle.**---Frontal onlap causes greater turbidity current run-up than lateral
615 onlap (Fig. 18B, C). This in turn makes the model presented here more applicable for dip sections against
616 a confining slope. This is further reinforced by the Le Ray dip-oblique correlation (Fig. 6), which is
617 interpreted to record the stratigraphic evolution of onlap described. The lack of a significant thin-bedded
618 slope drape at the lateral onlap of Grès d'Annot at Chalufy (e.g., Puigdefàbregas et al. 2004; Smith and
619 Joseph, 2004) may be an example of the importance of incidence angle, with run-up decreased against the
620 lateral slope (Fig. 18B, C).

621 A minor thin-bedded slope drape does exist at Chalufy, however, and intra-formational onlap
622 does occur against these thin beds (e.g., Bakke et al. 2013). This relationship may occur against lateral
623 margins because flows become increasingly elongate with increasing sediment concentrations (Al-Jaidi et
624 al. 2004). In strike sections this will result in a similar onlap termination pattern, with thicker and lower-

concentration flows of the lobe fringe depositing higher on the lateral slope than higher-concentration flows of the lobe axis, which are elongated in the dip direction and more prone to bypass down-dip. This relationship may therefore apply to both strike and dip exposures; however, greater understanding of frontal vs. lateral onlap in exposed or subsurface deep-water systems is required for further analysis.

The lack of a substantial thin-bedded drape at Chalufy may also be caused by its relatively distal position compared to the Annot Basin (Fig. 2), resulting in lower-velocity and lower-concentration flows being unable to maintain enough energy during their longer passage down the slope to deposit significant thicknesses of sediment high on the confining slopes (Fig. 20).

Hierarchical Scale.--- The onlap patterns observed in this study are seen mainly on the scale of tens of meters, similar to typical lobe or possibly lobe-complex dimensions (Prélat et al. 2009). Above the spatio-temporal scale of lobe complexes the morphology of the depositional element is less likely to be the result of autogenic processes acting on individual events and more likely to be controlled by allogenic factors, such as the interplay of basin subsidence and sediment supply (see stratigraphic interval scale of Sheets et al. 2002; Jobe et al. 2017) (Fig. 21). It should be noted that in confined basins established morphometric ranges for unconfined depositional element thicknesses break down due to variable degrees of confinement across systems (Prélat et al. 2010). The lobe-scale applicability of the model is therefore purely a hierarchical observation because lobe thicknesses will vary across systems.

Stratigraphic Position.--- Lobe progradation is unlikely to be constant; fluctuations in sediment supply, relative sea-level or changes in routing may result in small-scale backstepping. This backstepping creates discrete boundaries between successive members in the Annot Basin (Callec, 2004; Euzen et al. 2004) (Figs. 3, 5). These fluctuations will result in a non-uniform evolution of flow concentration during progradation, however on the basin-scale the overall trend of increasing flow concentration and subsequent onlap style will be maintained, with higher-density flows becoming more prevalent in the basin through progradation. These observations make the model most applicable to the early fill of confined deep-water systems, where confinement is greatest and distal thin-bedded turbidites will be most prevalent.

Low-density and thin-bedded turbidites also tend to form thinner successions than high-density and thick-bedded turbidites. This is because sediment volume and sedimentation rates are greater in higher-density flows and because differential compaction more heavily affects finer-grained successions. This has implications for the evolution of onlap because the distal lobe fringe will be thinner than the lobe axis. As a result, the intra-formational onlap against the underlying fringe will be much more difficult to detect through time as the draping low-density turbidites gradually become thinner as the basin fills, eventually resulting in the higher-density flows onlapping directly against the hemipelagic basin margin (Fig. 17). This relationship is seen in the Le Ray member (Fig. 6), where the thin-bedded fringe is gradually surmounted by later flows.

Other Variables.---This conceptual model aims to describe in simple terms the effect that autogenic flow evolution may have on onlap patterns in confined basins. Variables such as a waxing-waning sediment supply, hemipelagic aggradation rates, and the dominant grain size of the system are not discussed fully; however they will act to alter the autogenic processes that affect onlap and should be explored in future studies.

CONCLUSION

Understanding flow interaction with, and bed termination against, confining topography is critical for reconstructing the structural and sedimentological evolution of deep-water basins. This study presents a review of onlap styles in deep-water settings based on detailed field investigations and compares these results against those from a simple numerical model. Onlap terminations are shown to evolve in a predictable way through the progradation of a submarine lobe succession, with different lobe sub-environments identified at the basin margin through the migration of successive termination points and facies trends.

Initially termination points migrate towards the basin margins as low-density turbidites significantly drape the inherited basinal topography. Progressively higher-magnitude flows with greater sediment concentrations of the hybrid-bed-rich proximal fan fringe onlap these underlying deposits, causing the development of an intra-formational onlap surface that is characterized by either a basinward shift in termination points or a reduced distance between successive termination points towards the basin

678 margin. Hybrid beds are also shown to constitute significant thicknesses of the proximal fringe in
679 confined systems through long run-out transformation, slope-induced transformation, and intra-basinal
680 slope instability. Progradation of the lobe off-axis over the proximal fringe will cause further intra-
681 formational onlap as the lower-concentration off-axis deposits drape the slope. Onlap against the fringe
682 drape will continue until it is surmounted and onlap occurs directly against the hemipelagic basin margin.
683 Intra-formational onlap may also occur in the lobe axis through abrupt onlap of these high-concentration
684 deposits against the underlying lower-concentration fringe or off-axis deposits.

685 These sedimentological processes act to modulate the allogenic signals present in the Grès
686 d'Annot of the Annot Basin, with onlap patterns controlled by both allogenic processes, through tectonic
687 deformation and increasing sediment supply, and autogenic processes, through the interaction between
688 longitudinal flow evolution and confining basin margins. Depositional hierarchy is also shown to be
689 important when interpreting onlap patterns, with autogenic processes more important at the lobe scale
690 and allogenic processes more important at the lobe-complex scale.

691 **ACKNOWLEDGMENTS**

692 Soutter is funded by Natural Environment Research Council (NERC) grant number
693 NE/M00578X/1. Constructive reviews by B. Prather, Y. Spychala, and M. Mayall helped clarify both the
694 content and presentation of the manuscript, and are gratefully acknowledged. Associate Editor S.
695 Hubbard and Corresponding Editor J. Southard are thanked for editorial handling of the manuscript and
696 additional comments. Stereonet 10 is acknowledged for data plotting.

697 **REFERENCES**

698 Al Ja'Aidi, O.S., McCaffrey, W.D., and Kneller, B.C, 2004, Factors influencing the deposit geometry of
699 experimental turbidity currents: implications for sand-body architecture in confined basins, *in* Lomas, S.,
700 and Joseph, P., eds., Confined Turbidite Basins: Geological Society of London, Special Publication 222, p.
701 45–58.

702 Amy, L.A., McCaffrey, W.D., and Kneller, B.C., 2004, The influence of a lateral basin-slope on the
703 depositional patterns of natural and experimental turbidity currents, *in* Lomas, S., and Joseph, P., eds.,

704 Deep-Water Sedimentation in the Alpine Basin of SE France: New Perspectives on the Grès d'Annot and
705 Related Systems: Geological Society of London, Special Publication 221, p. 311-330.

706 Apps, G, 1987, Evolution of the Grès d'Annot Basin, SW Alps: Ph.D. thesis, University of Liverpool, 434
707 p.

708 Apps, G., Peel, F., and Elliott, T., 2004, The structural setting and palaeogeographical evolution of the
709 Grès d'Annot basin. *in* Lomas, S., and Joseph, P., eds., Deep-Water Sedimentation in the Alpine Basin of
710 SE France: New Perspectives on the Grès d'Annot and Related Systems: Geological Society of London,
711 Special Publication 221, p. 65-96.

712 Armitage, D.A., Romans, B.W., Covault, J.A. and Graham, S.A., 2009, The influence of mass-transport-
713 deposit surface topography on the evolution of turbidite architecture: The Sierra Contreras, Tres Pasos
714 Formation (Cretaceous), southern Chile: Journal of Sedimentary Research, v. 79, p. 287-301.

715 Azpiroz-Zabala, M., Cartigny, M.J., Talling, P.J., Parsons, D.R., Sumner, E.J., Clare, M.A., Simmons, S.M.,
716 Cooper, C., and Pope, E.L., 2017, Newly recognized turbidity current structure can explain prolonged
717 flushing of submarine canyons: Science Advances, v. 3, e1700200.

718 Baas, J.H., 2004, Conditions for formation of massive turbiditic sandstones by primary depositional
719 processes: Sedimentary Geology, v. 166, p. 293-310.

720 Baas, J.H., Best, J.L., and Peakall, J., 2011, Depositional processes, bedform development and hybrid bed
721 formation in rapidly decelerated cohesive (mud-sand) sediment flows: Sedimentology, v. 58, p. 1953-1987.

722 Bakke, K., Kane, I.A., Martinsen, O.J., Petersen, S.A., Johansen, T.A., Hustoft, S., Jacobsen F.H., and
723 GrotH, A., 2013, Seismic modeling in the analysis of deep-water sandstone termination styles: American
724 Association of Petroleum Geologists, Bulletin, v. 97, p. 1395-1419.

725 Barker, S.P., Haughton, P.D.W., McCaffrey, W.D., Archer, S.G., and Hakes, B, 2008, Development of
726 rheological heterogeneity in clay-rich high-density turbidity currents: Aptian Britannia Sandstone
727 Member, UK continental shelf: Journal of Sedimentary Research, v. 78, p. 45–68.

728 Beaubouef, R.T., and Friedmann, S.J., 2000, High resolution seismic/sequence stratigraphic framework
729 for the evolution of Pleistocene intra slope basins, western Gulf of Mexico: depositional models and
730 reservoir analogs, in: Deep-Water Reservoirs of the World: Gulf Coast Section SEPM 20th Annual
731 Research Conference, p. 40-60.

732 Bell, D., Kane, I.A., Pontén, A.S., Flint, S.S., Hodgson, D.M., and Barrett, B.J., 2018a, Spatial variability in
733 depositional reservoir quality of deep-water channel-fill and lobe deposits: Marine and Petroleum
734 Geology, v. 98, p. 97-115.

735 Bell, D., Stevenson, C.J., Kane, I.A., Hodgson, D.M. and Poyatos-Moré, M., 2018b, Topographic controls
736 on the development of contemporaneous but contrasting basin-floor depositional architectures: Journal
737 of Sedimentary Research, v. 88, p. 1166-1189.

738 Boulesteix, K., Poyatos-More, M., Flint, S.S., Taylor, K., Hodgson, D.M., and Hasiotis, T. M., 2019a,
739 Transport and deposition of mud in deep-water environments: processes and stratigraphic implications:
740 Sedimentology, in press

741 Boulesteix, K., Poyatos-Moré, M., Flint, S., Hodgson, D.M., Taylor, K.G., and Parry, G.R. 2019b,
742 Sedimentary facies and stratigraphic architecture of deep-water mudstones beyond the basin-floor fan
743 sandstone pinchout: EarthArXiv.

744 Bouma, A.H., 1962, Sedimentology of Some Flysch Deposits; A Graphic Approach to Facies
745 Interpretation: New York, Elsevier, 168 p.

746 Brunt, R.L., McCaffrey, W.D., and Kneller, B.C., 2004, Experimental modeling of the spatial distribution
747 of grain size developed in a fill-and-spill mini-basin setting: Journal of Sedimentary Research, v. 74, p.
748 438-446.

749 Callec, Y., 2004, The turbidite fill of the Annot sub-basin (SE France): a sequence-stratigraphy approach,
750 *in* Lomas, S., and Joseph, P., eds., Deep-Water Sedimentation in the Alpine Basin of SE France: New
751 Perspectives on the Grès d'Annot and Related Systems: Geological Society of London, Special
752 Publication 221, p. 111-135.

753 Clare, M.A., Talling, P.J., Challenor, P., Malgesini, G., and Hunt, J., 2014, Distal turbidites reveal a
754 common distribution for large (> 0.1 km^3) submarine landslide recurrence: Geology, v. 42, p. 263-266.

755 Clark, J.D., and Stanbrook, A., 2001, Formation of large-scale shear structures during deposition from
756 high-density turbidity currents, Grès d'Annot Formation, south-east France: Particulate Gravity
757 Currents, v. 31, p. 219-232.

758 Covault, J.A., and Romans, B.W., 2009, Growth patterns of deep-sea fans revisited: Turbidite-system
759 morphology in confined basins, examples from the California Borderland: Marine Geology, v. 265, p. 51-
760 66.

761 Cunha, R.S., Tinterri, R., and Magalhaes, P.M., 2017, Annot Sandstone in the Peïra Cava basin: An
762 example of an asymmetric facies distribution in a confined turbidite system (SE France). Marine and
763 Petroleum Geology, v. 87, p. 60-79.

764 Deptuck, M.E., Piper, D.J., Savoye, B., and Gervais, A., 2008, Dimensions and architecture of late
765 Pleistocene submarine lobes off the northern margin of East Corsica: Sedimentology, v. 55, p. 869-898.

766 DeVries, M., and Lindholm, R.M., 1994, Internal architecture of a channel– levee complex, Cerro Toro
767 Formation, Southern Chile, *in* Weimer, P., Bouma, A.H., and Perkins, B.F., eds., Submarine Fans and
768 Turbidite Systems: Gulf Coast Section SEPM Foundation, Houston, p. 105–114.

769 Dorrell, R.M., Patacci, M., and McCaffrey, W. D., 2019, Inflation of ponded, particulate-laden density
770 currents: Journal of Sedimentary Research, v. 88, p. 1276–1282.

771 Doughty-Jones, G., Mayall, M., and Lonergan, L., 2017, Stratigraphy, facies, and evolution of deep-water
772 lobe complexes within a salt-controlled intraslope minibasin: American Association of Petroleum
773 Geologists, Bulletin, v. 101, p. 1879-1904.

774 Du Fornel, E., Joseph, P., Desaubliaux, G., Eschard, R., Guillocheau, F., Lerat, O., Muller, C., Ravenne,
775 C., and Sztrakos, K., 2004, The southern Grès d'Annot outcrops (French Alps): an attempt at regional
776 correlation, *in* Lomas, S., and Joseph, P., eds., Deep-Water Sedimentation in the Alpine Basin of SE

777 France: New Perspectives on the Grès d'Annot and Related Systems: Geological Society of London,
778 Special Publication 221, p. 137-160.

779 Eggenhuisen, J.T., McCaffrey, W.D., Haughton, P.D., and Butler, R.W., 2011, Shallow erosion beneath
780 turbidity currents and its impact on the architectural development of turbidite sheet
781 systems: Sedimentology, v. 58, p. 936-959.

782 Eggenhuisen, J.T., Cartigny, M.J., and de Leeuw, J., 2017, Physical theory for near-bed turbulent particle
783 suspension capacity: Earth Surface Dynamics, v. 5, p. 269-281.

784 Elliott, T., Apps, G., Davies, H., Evans, M., Ghibaudo, G., and Graham, R.H., 1985, A structural and
785 sedimentological traverse through the Tertiary foreland basin of the external Alps of south-east France, *in*
786 Field Excursion Guidebook for the International Association of Sedimentologists Meeting on Foreland
787 Basins in Fribourg, eds., Allen, P.A., and Homewood, P, p. 39-73.

788 Euzen, T., Joseph, P., Du Fornel, E., Lesur, S., Granjeon, D., and Guillocheau, F., 2004, Three-
789 dimensional stratigraphic modelling of the Grès d'Annot system, Eocene-Oligocene, SE France, *in*
790 Lomas, S., and Joseph, P., eds., Deep-Water Sedimentation in the Alpine Basin of SE France: New
791 Perspectives on the Grès d'Annot and Related Systems: Geological Society of London, Special
792 Publication 221, p. 161-180.

793 Gardiner, A.R., 2006, The variability of turbidite sandbody pinchout and its impact on hydrocarbon
794 recovery in stratigraphically trapped fields, *in* The Deliberate Search for the Stratigraphic Trap, eds., Allen,
795 M.R., Goffey, G.P., Morgan, R.K., and Walker, I.M. Geological Society of London, Special Publications
796 254, p. 267-287.

797 Gervais, A., Savoye, B., Piper, D.J., Mulder, T., Cremer, M., and Pichevin, L., 2004, Present morphology
798 and depositional architecture of a sandy confined submarine system: the Golo turbidite system (eastern
799 margin of Corsica, *in* Lomas, S., and Joseph, P., eds., Confined Turbidite Basins: Geological Society of
800 London, Special Publication 222,, p. 59-89.

801 Grecula, M., Flint, S., Potts, G., Wickens, D. and Johnson, S., 2003, Partial ponding of turbidite systems
802 in a basin with subtle growth-fold topography: Laingsburg-Karoo, South Africa: Journal of Sedimentary
803 Research, v. 73, p. 603-620.

804 Groenenberg, R.M., Hodgson, D.M., Prelat, A., Luthi, S.M., and Flint, S.S., 2010, Flow-deposit
805 interaction in submarine lobes: Insights from outcrop observations and realizations of a process-based
806 numerical model: Journal of Sedimentary Research, v. 80, p. 252-267.

807 Grundvåg, S.A., Johannessen, E.P., Helland-Hansen, W., and Plink-Björklund, P., 2014, Depositional
808 architecture and evolution of progradationally stacked lobe complexes in the Eocene Central Basin of
809 Spitsbergen: Sedimentology, v. 61, p. 535-569.

810 Hansen, L.A.S., Hodgson, D.M., Pontén, A., Bell, D., and Flint, S., 2019, Quantification of basin-floor
811 fan pinchouts: examples from the Karoo Basin, South Africa: Frontiers in Earth Science, v. 7. 12 p.

812 Haughton, P.D.W., 1994, Deposits of deflected and ponded turbidity currents, Sorbas basin, Southeast
813 Spain: Journal of Sedimentary Petrology, v. B64, p. 233–246.

814 Haughton, P.D., 2000, Evolving turbidite systems on a deforming basin floor, Tabernas, SE
815 Spain: Sedimentology, v. 47, p. 497-518.

816 Haughton, P.D., Barker, S.P., and McCaffrey, W.D., 2003, 'Linked' debrites in sand-rich turbidite systems
817 - origin and significance: Sedimentology, v. 50, p. 459-482.

818 Haughton, P., Davis, C., McCaffrey, W., and Barker, S., 2009, Hybrid sediment gravity flow deposits -
819 classification, origin and significance: Marine and Petroleum Geology, v. 26, p. 1900-1918.

820 Hiscott, R.N., 1994, Loss of capacity, not competence, as the fundamental process governing deposition
821 from turbidity currents: Journal of Sedimentary Petrology, v. 64, p. 209–214.

822 Hodgson, N.A., Farnsworth, J., and Fraser, A.J., 1992, Salt-related tectonics, sedimentation and
823 hydrocarbon plays in the Central Graben, North Sea, UKCS: *in* Hardman, R.F.P., eds., Exploration

824 Britain: Geological Insights for the Next Decade: Geological Society of London, Special Publication 67,
825 p. 31-63.

826 Hodgson, D.M., Flint, S.S., Hodgetts, D., Drinkwater, N.J., Johannessen, E.P., and Luthi, S.M., 2006,
827 Stratigraphic evolution of fine-grained submarine fan systems, Tanqua depocenter, Karoo Basin, South
828 Africa: Journal of Sedimentary Research, v. 76, p. 20-40.

829 Hodgson, D.M., 2009, Distribution and origin of hybrid beds in sand-rich submarine fans of the Tanqua
830 depocenter, Karoo Basin, South Africa: Marine and Petroleum Geology, v. 26, p. 1940-1956.

831 Hodgson, D.M., and Haughton, P.D., 2004, Impact of syndepositional faulting on gravity current
832 behaviour and deep-water stratigraphy: Tabernas-Sorbas Basin, SE Spain, *in* Lomas, S., and Joseph, P.,
833 eds., Confined Turbidite Basins: Geological Society of London, Special Publication 222, p. 135-158.

834 Fonnesu, M., Haughton, P., Felletti, F., and McCaffrey, W., 2015, Short length-scale variability of hybrid
835 event beds and its applied significance: Marine and Petroleum Geology, v. 67, p. 583-603.

836 Fonnesu, M., Felletti, F., Haughton, P.D., Patacci, M., and McCaffrey, W.D., 2018, Hybrid event bed
837 character and distribution linked to turbidite system sub-environments: the North Apennine Gottero
838 Sandstone (north-west Italy): Sedimentology, v. 65, p. 151-190.

839 Ford, M., Lickorish, W., and Kusnir, N., 1999, Tertiary foreland sedimentation in the southern subalpine
840 chains, SE France: a geodynamic appraisal: Basin Research, v. 11, p. 315-336.

841 Kane, I.A., McCaffrey, W.D., and Martinsen, O.J., 2009, Allogenic vs. autogenic controls on megaflute
842 formation: Journal of Sedimentary Research, v. 79, p. 643-651.

843 Kane, I.A., Catterall, V., McCaffrey, W.D., and Martinsen, O.J., 2010, Submarine channel response to
844 intrabasinal tectonics: the influence of lateral tilt: American Association of Petroleum Geologists,
845 Bulletin, v. 94, p. 189-219.

846 Kane, I.A. and Pontén, A.S., 2012, Submarine transitional flow deposits in the Paleogene Gulf of
847 Mexico: Geology, v. 40, p. 1119-1122.

Kane, I.A., McGee, D.T., and Jobe, Z.R., 2012, Halokinetic effects on submarine channel equilibrium profiles and implications for facies architecture: conceptual model illustrated with a case study from Magnolia Field, Gulf of Mexico, *in* Alsop G.I et al., eds., Salt Tectonics, Sediment and Prospectivity: Geological Society of London, Special Publication 363, p. 289-302.

Kane, I.A., Pontén, A.S., Vangdal, B., Eggenhuisen, J.T., Hodgson, D.M., and Spychala, Y.T., 2017, The stratigraphic record and processes of turbidity current transformation across deep-marine lobes: Sedimentology, v. 64, p. 1236-1273.

Kilhams, B., Hartley, A., Huuse, M., and Davis, C., 2012, Characterizing the Paleocene turbidites of the North Sea: the Mey Sandstone Member, Lista Formation, UK Central Graben. Petroleum Geoscience, v. 18, p. 337-354.

Kneller, B.C., Edwards, D., McCaffrey, W.D., and Moore, R., 1991, Oblique reflection of turbidity currents: Geology, v. 19, p. 250 252.

Kneller, B. C., 1995, Beyond the turbidite paradigm: physical models for deposition of turbidites and their implications for reservoir prediction. *in* Hartley, A., and Prosser, D.J., eds., Characterisation of Deep Marine Clastic Systems: Geological Society of London, Special Publications 94, p. 29-46.

Kneller, B.C., and McCaffrey, W.D., 1995, Modelling the effects of salt-induced topography on deposition from turbidity currents: SEPM, Gulf Coast Section, p. 137-145.

Kneller, B. C., and McCaffrey, W. D., 1999, Depositional effects of flow non-uniformity and stratification within turbidity currents approaching a bounding slope: deflection, reflection and facies variation: Journal of Sedimentary Research, v. 69, p. 980-991.

Kneller, B., Dykstra, M., Fairweather, L., and Milana, J.P., 2016, Mass-transport and slope accommodation: implications for turbidite sandstone reservoirs: American Association of Petroleum Geologists, Bulletin, v. 100, p. 213-235.

Kubo, Y.S., 2004, Experimental and numerical study of topographic effects on deposition from two-dimensional, particle-driven density currents: Sedimentary Geology, v. 164, p. 311-326.

873 Jackson, C.A.L., Barber, G.P., and Martinsen, O.J., 2008, Submarine slope morphology as a control on
874 the development of sand-rich turbidite depositional systems: 3D seismic analysis of the Kyrre Fm (Upper
875 Cretaceous), Måløy Slope, offshore Norway: Marine and Petroleum Geology, v. 25, p. 663-680.

876 Jackson, C.A.L., Zakaria, A.A., Johnson, H.D., Tongkul, F., and Crevello, P.D., 2009, Sedimentology,
877 stratigraphic occurrence and origin of linked debrites in the West Crocker Formation (Oligo-Miocene),
878 Sabah, NW Borneo: Marine and Petroleum Geology, v. 26, p. 1957-1973.

879 Jobe, Z.R., Sylvester, Z., Howes, N., Pirmez, C., Parker, A., Cantelli, A., Smith, R., Wolinsky, M.A.,
880 O'Byrne, C., Slowey, N., and Prather, B., 2017, High-resolution, millennial-scale patterns of bed
881 compensation on a sand-rich intraslope submarine fan, western Niger Delta slope: Geological Society of
882 America, Bulletin, v. 129, p. 23-37.

883 Joseph, P., and Lomas, S.A., 2004, Deep-water sedimentation in the Alpine Foreland Basin of SE France:
884 New perspectives on the Grès d'Annot and related systems—an introduction: Geological Society,
885 London, Special Publications, v. 221, p. 1-16.

886 Lamb, M.P., Parsons, J.D., Mullenbach, B.L., Finlayson, D.P., Orange, D.L., and Nittrouer, C.A., 2008,
887 Evidence for superelevation, channel incision, and formation of cyclic steps by turbidity currents in Eel
888 Canyon, California: Geological Society of America Bulletin, v. 120, p. 463-475.

889 Lee, S.E., Amy, L.A., and Talling, P.J., 2004, The character and origin of thick base-of-slope sandstone
890 units of the Peïra Cava outlier, SE France, *in* Lomas, S., and Joseph, P., eds., Deep-Water Sedimentation
891 in the Alpine Basin of SE France: New Perspectives on the Grès d'Annot and Related Systems:
892 Geological Society of London, Special Publication 221, p. 331-347.

893 Liu, Q., Kneller, B., Fallgatter, C., Valdez Buso, V., and Milana, J.P., 2018, Tabularity of individual
894 turbidite beds controlled by flow efficiency and degree of confinement: Sedimentology, v. 65, p. 2368 -
895 2387.

896 Lomas, S.A., and Joseph, P., 2004, Confined turbidite systems, *in* Lomas, S., and Joseph, P., eds.,
897 Confined Turbidite Basins: Geological Society of London, Special Publication 222, p. 1-7.

898 Lowe, D.R., 1982, Sediment gravity flows: II Depositional models with special reference to the deposits
899 of high-density turbidity currents: Journal of Sedimentary Petrology, v. 52. p. 279-297.

900 Lowe, D.R., and Guy, M., 2000, Slurry-flow deposits in the Britannia Formation (Lower Cretaceous),
901 North Sea: a new perspective on the turbidity current and debris flow problem: Sedimentology, v. 47, p.
902 31-70.

903 Marini, M., Milli, S., Ravnås, R., and Moscatelli, M., 2015, A comparative study of confined vs. semi-
904 confined turbidite lobes from the Lower Messinian Laga Basin (Central Apennines, Italy): implications
905 for assessment of reservoir architecture: Marine and Petroleum Geology, v. 63, p. 142-165.

906 Marini, M., Patacci, M., Felletti, F., and McCaffrey, W.D., 2016, Fill to spill stratigraphic evolution of a
907 confined turbidite mini-basin succession, and its likely well bore expression: The Castagnola Fm, NW
908 Italy: Marine and Petroleum Geology, v. 69, p. 94-111.

909 Mayall, M., Lonergan, L., Bowman, A., James, S., Mills, K., Primmer, T., Pope, D., Rogers, L., and
910 Skeene, R., 2010, The response of turbidite slope channels to growth-induced seabed
911 topography: American Association of Petroleum Geologists, Bulletin, v. 94, p. 1011-1030.

912 McCaffrey, W.D., and Kneller, B.C., 2001, Process controls on the development of stratigraphic trap
913 potential on the margins of confined turbidite systems and aids to reservoir evaluation: American
914 Association of Petroleum Geologists, Bulletin, v. 85, p. 971-988.

915 McCaffrey, W.D., and Kneller, B.C., 2004, Scale effects of non-uniformity on deposition from turbidity
916 currents with reference to the Gres d'Annot of SE France, *in* Lomas, S., and Joseph, P., eds., Deep-Water
917 Sedimentation in the Alpine Basin of SE France: New Perspectives on the Grès d'Annot and Related
918 Systems: Geological Society of London, Special Publication 221, p. 301-310.

919 Middleton, G.V., and Hampton, M.A., 1973, Sediment gravity flows: Mechanics of flow and deposition,
920 *in* Middleton, G.V., Bouma, A.H., eds., Turbidites and Deep Water Sedimentation: Pacific Section,
921 Society of Economic Paleontologists and Mineralogists Book 2, Short Course Notes, p. 1–38.

922 Mohrig, D., and Buttles, J., 2007, Deep turbidity currents in shallow channels: Geology, v. 35, p. 155-158.

923 Mougin, F., 1978, Contribution à l'étude des Sédiments tertiaires de la partie orientale du synclinal
924 d'Annot (Alpes de Haute Provence). Stratigraphie, Grochimie, Micropaldontologie: Unpublished Ph.D.
925 Thesis, Université Scientifique et Médicale de Grenoble, Grenoble. 165 p.

926 Muck, M.T., and Underwood, M.B., 1990, Upslope flow of turbidity currents: a comparison among field
927 observations, theory, and laboratory models: Geology, v. 18, p. 54-57

928 Mulder, T., and Alexander, J., 2001, The physical character of subaqueous sedimentary density flows and
929 their deposits: Sedimentology, v. 48, p. 269-299.

930 Mutti, E., Bernoulli, D., Ricci Lucchi, F., and Tinterri, R., 2009, Turbidites and turbidity currents from
931 Alpine 'flysch' to the exploration of continental margins: Sedimentology, v. 56, p. 267-318.

932 Oluboyo, A.P., Gawthorpe, R.L., Bakke, K., and Hadler-Jacobsen, F., 2014, Salt tectonic controls on
933 deep-water turbidite depositional systems: Miocene, southwestern Lower Congo Basin, offshore
934 Angola: Basin Research, v. 26, p. 597-620.

935 Ortiz-Karpf, A., Hodgson, D.M., and McCaffrey, W.D., 2015, The role of mass-transport complexes in
936 controlling channel avulsion and the subsequent sediment dispersal patterns on an active margin: the
937 Magdalena Fan, offshore Colombia: Marine and Petroleum Geology, v. 64, p. 58-75.

938 Ortiz-Karpf, A., Hodgson, D.M., Jackson, C.A.L., and McCaffrey, W.D., 2016, Mass-transport complexes
939 as markers of deep-water fold-and-thrust belt evolution: insights from the southern Magdalena Fan,
940 Offshore Colombia: Basin Research, v. 30, p. 65-88.

941 Patacci, M., Haughton, P.D., and McCaffrey, W.D., 2014, Rheological complexity in sediment gravity
942 flows forced to decelerate against a confining slope, Braux, SE France: Journal of Sedimentary
943 Research, v. 84, p. 270-277.

944 Pickering, K.T., and Hiscott, R.N., 1985, Contained (reflected) turbidity currents from the Middle
945 Ordovician Cloridorme Formation, Quebec, Canada: an alternative to the antidune
946 hypothesis: Sedimentology, v. 32, p. 373-394.

947 Pinter, P.R., Butler, R.W., Hartley, A.J., Maniscalco, R., Baldassini, N., and Di Stefano, A., 2017, Tracking
948 sand-fairways through a deformed turbidite system: the Numidian (Miocene) of Central Sicily, Italy: Basin
949 Research, v. 30, p. 480-501.

950 Piper, D.J., Cochonat, P., and Morrison, M.L., 1999, The sequence of events around the epicentre of the
951 1929 Grand Banks earthquake: initiation of debris flows and turbidity current inferred from sidescan
952 sonar: Sedimentology, v. 46, p. 79-97.

953 Prather, B.E., Booth, J.R., Steffens, G.S., and Craig, P. A., 1998, Classification, lithologic calibration, and
954 stratigraphic succession of seismic facies of intraslope basins, deep-water Gulf of Mexico:. American
955 Association of Petroleum Geologists, Bulletin, v. 82, p. 701-728.

956 Prather, B.E., Pirmez, C., and Winker, C.D., 2012, Stratigraphy of linked intraslope basins: Brazos-Trinity
957 system western Gulf of Mexico, *in* Prather B.E. et al., eds., Application of the Principles of Seismic
958 Geomorphology to Continental-Slope and Base-of-Slope Systems: Case Studies from Seafloor and Near-
959 Seafloor Analogues: SEPM, Special Publication 99, p. 83-109.

960 Prather, B.E., O'Byrne, C., Pirmez, C., and Sylvester, Z., 2017, Sediment partitioning, continental slopes
961 and base-of-slope systems: Basin Research, v. 29, p. 394-416.

962 Prélat, A., Hodgson, D.M., and Flint, S.S., 2009, Evolution, architecture and hierarchy of distributary
963 deep-water deposits: a high-resolution outcrop investigation from the Permian Karoo Basin, South
964 Africa: Sedimentology, v. 56, p. 2132-2154.

965 Prélat, A., Covault, J.A., Hodgson, D.M., Fildani, A., and Flint, S.S., 2010, Intrinsic controls on the range
966 of volumes, morphologies, and dimensions of submarine lobes: Sedimentary Geology, v. 232, p. 66-76.

967 Puigdefàbregas, C., Gjelberg, J.M., and Vaksdal, M., 2004, The Grès d'Annot in the Annot syncline: outer
968 basin-margin onlap and associated soft-sediment deformation, *in* Lomas, S., and Joseph, P., eds., Deep-
969 Water Sedimentation in the Alpine Basin of SE France: New Perspectives on the Grès d'Annot and
970 Related Systems: Geological Society of London, Special Publication 221, p. 367-388.

971 Ravenne, C., Riche, P., Tremolieres, P., and Vially, R., 1987, Sédimentation et tectonique dans le bassin
972 marin Eocène supérieur-Oligocène des Alpes du Sud: Revue de Institut Français du Pétrole, v. 42, p. 529-
973 553.

974 Salles, L., Ford, M., Joseph, P., De Veslud, C.L.C., and Le Solleuz, A., 2011, Migration of a synclinal
975 depocenter from turbidite growth strata: the Annot syncline, SE France: Bulletin de la Société Géologique
976 de France, v. 182, p. 199-220.

977 Salles, L., Ford, M., and Joseph, P., 2014, Characteristics of axially-sourced turbidite sedimentation on an
978 active wedge-top basin (Annot Sandstone, SE France): Marine and Petroleum Geology, v. 56, p. 305-323.

979 Sheets, B.A., Hickson, T.A., and Paola, C., 2002, Assembling the stratigraphic record: depositional
980 patterns and time-scales in an experimental alluvial basin: Basin Research, v. 14, p. 287-301.

981 Sinclair, H.D., 1994, The influence of lateral basin slopes on turbidite sedimentation in the Annot
982 Sandstones of SE France: Journal of Sedimentary Petrology, v. B64, p. 42-54.

983 Sinclair, H.D., 1997, Tectonostratigraphic model for underfilled peripheral foreland basins: An Alpine
984 perspective: Geological Society of America, Bulletin, v. 109, p. 324-346

985 Sinclair, H.D., 2000, Delta-fed turbidites infilling topographically complex basins: a new depositional
986 model for the Annot Sandstones, SE France: Journal of Sedimentary Research, v. 70, p. 504–519.

987 Sinclair, H.D., and Tomasso, M., 2002, Depositional evolution of confined turbidite basins: Journal of
988 Sedimentary Research, p. 72, v. 451-456.

989 Sømme, T.O., Piper, D.J., Deptuck, M.E., and Helland-Hansen, W., 2011, Linking onshore-offshore
990 sediment dispersal in the Golo source-to-sink system (Corsica, France) during the late
991 Quaternary: Journal of Sedimentary Research, v. 81, p. 118-137.

992 Southern, S.J., Patacci, M., Felletti, F., and McCaffrey, W.D., 2015, Influence of flow containment and
993 substrate entrainment upon sandy hybrid event beds containing a co-genetic mud-clast-rich
994 division: Sedimentary Geology, p. 321, v. 105-122.

995 Soutter, E.L., Kane, I.A., and Huuse, M., 2018, Giant submarine landslide triggered by Paleocene mantle
996 plume activity in the North Atlantic: Geology, v. 46, p. 511-514.

997 Stanbrook, D.A., and Clark, J.D., 2004, The Marnes Brunes Inférieures in the Grand Coyer remnant:
998 characteristics, structure and relationship to the Grès d'Annot, *in* Lomas, S., and Joseph, P., eds., Deep-
999 Water Sedimentation in the Alpine Basin of SE France: New Perspectives on the Grès d'Annot and
1000 Related Systems: Geological Society of London, Special Publication 221, v. 285-300.

1001 Stanley, D.J., and Mutti, E., 1968, Sedimentological evidence for an emerged land mass in the Ligurian sea
1002 during the Palaeogene: Nature, v. 218, p 32.

1003 Stanley, D.J., 1980, The Saint-Antonin conglomerate in the Maritime Alps: a model for coarse
1004 sedimentation on a submarine slope: Smithsonian Contributions to the Marine Sciences, v. 5, p. 1–25.

1005 Smith, R.U., 2004a, Silled sub-basins to connected tortuous corridors: sediment distribution systems on
1006 topographically complex sub-aqueous slopes, *in* Lomas, S., and Joseph, P., eds., Confined Turbidite
1007 Basins: Geological Society of London, Special Publication 222, p. 23-43.

1008 Smith, R., 2004b, Turbidite systems influenced by structurally induced topography in the multi-sourced
1009 Welsh Basin, *in* Lomas, S., and Joseph, P., eds., Confined Turbidite Basins: Geological Society of London,
1010 Special Publication 222, p. 209-228.

1011 Smith, R., and Joseph, P., 2004, Onlap stratal architectures in the Grès d'Annot: Geometric models and
1012 controlling factors, *in* Lomas, S., and Joseph, P., eds., Deep-Water Sedimentation in the Alpine Basin of
1013 SE France: New Perspectives on the Grès d'Annot and Related Systems: Geological Society of London,
1014 Special Publication 221, p. 389-399

1015 Spychala, Y.T., Hodgson, D.M., Flint, S.S., and Mountney, N.P., 2015, Constraining the sedimentology
1016 and stratigraphy of submarine intraslope lobe deposits using exhumed examples from the Karoo Basin,
1017 South Africa: Sedimentary Geology, v. 322, p. 67-81.

1018 Spychala, Y.T., Hodgson, D.M., Stevenson, C.J., and Flint, S.S., 2016, Aggradational lobe fringes: The
1019 influence of subtle intrabasinal seabed topography on sediment gravity flow processes and lobe stacking
1020 patterns: Sedimentology, v. 64, p. 582-608.

1021 Spychala, Y.T., Hodgson, D.M., Prélat, A., Kane, I.A., Flint, S.S., and Mountney, N.P., 2017, Frontal and
1022 lateral submarine lobe fringes: comparing sedimentary facies, architecture and flow processes: Journal of
1023 Sedimentary Research, v. 87, p. 75-96.

1024 Spychala, Y., Eggenhuisen, J., Tilston, M., and Pohl, F., 2019, The influence of basin settings and flow
1025 properties on the dimensions of submarine lobe elements: EarthArXiv.

1026 Stevenson, C.J., Jackson, C.A.L., Hodgson, D.M., Hubbard, S.M., and Eggenhuisen, J.T., 2015, Deep-
1027 water sediment bypass: Journal of Sedimentary Research, v. 85, p. 1058-1081.

1028 Stevenson, C.J., Feldens, P., Georgiopoulou, A., Schönke, M., Krastel, S., Piper, D.J., Lindhorst, K., and
1029 Mosher, D., 2018, Reconstructing the sediment concentration of a giant submarine gravity flow: Nature
1030 communications, v. 9, 2616.

1031 Straub, K.M., Mohrig, D., McElroy, B., Buttles, J., and Pirmez, C., 2008, Interactions between turbidity
1032 currents and topography in aggrading sinuous submarine channels: a laboratory study: GSA Bulletin, v.
1033 120, p. 368-385.

1034 Sylvester, Z., Cantelli, A., and Pirmez, C., 2015, Stratigraphic evolution of intraslope minibasins: Insights
1035 from surface-based model: American Association of Petroleum Geologists, Bulletin, v. 99, p. 1099-1129.

1036 Symons, W.O., Sumner, E.J., Paull, C.K., Cartigny, M.J., Xu, J.P., Maier, K.L., Lorenson, T.D., and
1037 Talling, P.J., 2017, A new model for turbidity current behavior based on integration of flow monitoring
1038 and precision coring in a submarine canyon: Geology, v. 45, p. 367-370.

1039 Talling, P.J., Amy, L.A., and Wynn, R.B., 2007, New insight into the evolution of large-volume turbidity
1040 currents: comparison of turbidite shape and previous modelling results: Sedimentology, v. 54, p.737-769.

1041 Tinterri, R., Magalhaes, P.M., Tagliaferri, A., and Cunha, R.S., 2016, Convolute laminations and load
1042 structures in turbidites as indicators of flow reflections and decelerations against bounding slopes.

1043 Examples from the Marnoso-arenacea Formation (northern Italy) and Annot Sandstones (south eastern
1044 France): Sedimentary Geology, v. 344, p. 382-407.

1045 Tő kés, L., and Patacci, M., 2018, Quantifying tabularity of turbidite beds and its relationship to the
1046 inferred degree of basin confinement: Marine and Petroleum Geology, v. 97, p. 659- 671.

1047 Tomasso, M., and Sinclair, H.D., 2004, Deep-water sedimentation on an evolving fault-block: the Braux
1048 and St Benoit outcrops of the Grès d'Annot, *in* Lomas, S., and Joseph, P., eds., Deep-Water
1049 Sedimentation in the Alpine Basin of SE France: New Perspectives on the Grès d'Annot and Related
1050 Systems: Geological Society of London, Special Publication 221, p. 267-283.

1051 Walther, J., 1894, Einleitung in die Geologie als historische Wissenschaft, *in* Lithogenesis der Gegenwart.
1052 Jena, G. Fischer, v. 3, p. 535–1055.

1053 Weimer, P., and Link, M.H., 1991, Global petroleum occurrences in submarine fans and turbidite
1054 systems, *in* Weimer P., and Link M.H., eds., Seismic Facies and Sedimentary Processes of Submarine Fans
1055 and Turbidite Systems: Frontiers in Sedimentary Geology, New York, Springer, p. 9-67.

1056 Wilson, D., Davies, J.R., Waters, R.A., and Zalasiewiczt, J.A., 1992, A fault-controlled depositional model
1057 for the Aberystwyth Grits turbidite system: Geological Magazine, v. 129, p. 595-607.

1058 Wynn, R.B., Masson, D.G., Stow, D.A., and Weaver, P.P., 2000, The Northwest African slope apron: a
1059 modern analogue for deep-water systems with complex seafloor topography: Marine and Petroleum
1060 Geology, v. 17, p. 253-265.

1061 **FIGURE CAPTIONS**

1062 **Fig. 1: A)** Examples of onlap termination styles (modified from Al-Jaidi et al. 2004; Bakke et al. 2013;
1063 Patacci et al. 2014). **B)** Generalized relationship between flow concentration and onlap geometry
1064 (modified from Bakke et al. 2013). t = time.

1065 **Fig. 2:** Location and geological setting of the Cenozoic foreland basin of the Western Alps. The
1066 generalized Late Eocene paleogeography is overlaid (modified from Joseph and Lomas, 2004 and Salles et
1067 al. 2014) and shows the Annot Basin (red box) situated in a clastic deep-marine environment.. Red line
1068 indicates boundary between terrestrial and marine environments. RFZ, Rouaine Fault Zone. Blue arrows
1069 indicate paleoflow, and blue lines indicate schematic fluvial systems.

1070 **Fig. 3:** Structure, chronostratigraphy, and geological map of the Annot Basin (modified from
1071 Puigdefàbregas et al., 2004; Du Fornel et al. 2004; Salles et al. 2014). The various anticlines confine
1072 deposition across the Basin. The clastic sequence has been divided into members based on aerial and

outcrop mapping (modified from Puigdefàbregas et al., 2004; Salles et al., 2014). An attempt has been made to reconcile the member subdivisions used by Puigdefàbregas et al. (2004) and Salles et al. (2014). White boxes indicate logged localities. White lines indicate correlation panels in Fig. 5 and Fig. 6. RFZ, Rouaine Fault Zone; BF, Braux Fault. Black dashed lines indicate exhumed syn-sedimentary fault escarpments.

Fig. 4: A) Dip and B) strike field sketches of the stratigraphy and structure of the Annot Basin. Logged localities are shown as red traverses in part A.

Fig. 5: Dip-oblique correlation panel along the eastern margin of the Annot Basin. No horizontal scale. Localities and panel orientation are shown in Fig. 3. Members have been correlated based on published maps and lithological observations. Paleocurrent data are associated with one sedimentary log or series of logs from one locality. The vertical thickness represents the exposed stratigraphy along the correlated margin (see Fig. 3 for location) and does not represent the accommodation of the entire basin, which had a westward-migrating depocenter. This migration is represented in the eastern exposures by decreasing member thicknesses through time. It should also be noted that the due to the oblique nature of the correlation the margin position is a representation of the relative confinement at the member scale and does not indicate onlap angle.

Fig. 6: Correlation panel for the Le Ray member in the Annot Basin. Paleoflow is from the left to right (south to north). Inset shows 3D orientation of panel. BF, Braux Fault; SB, Saint-Benoît; LM, Le Marc; CF, Col du Fa.

Fig. 7: Correlation panel from the Col du Fa outcrop. The thinner-bedded low-density turbidites drape and heal the topography of the Marnes Bleues basin margin onlap surface, while the higher-density and thicker-bedded turbidites initially onlap against these distal deposits, forming an intra-formational onlap surface. Red lines on the horizontal axis indicate exact log position. Log key on Fig. 6.

Fig. 8: A) Nomenclature comparison between unconfined lobe sub-environments (Spychala et al. 2017) and **B)** confined lobe sub-environments. The only difference is that hybrid beds are more prevalent in lateral positions in confined systems due to rapid flow deceleration and transformation at basin margins. LDT = low-density turbidite; HEB = hybrid (event) bed; MDT = medium-density turbidite; HDT = high-density turbidite. Unconfined and confined lobe dimensions are from Prelat et al. (2010).

Fig. 9: Sedimentary logs with facies and paleogeographical interpretations. Each member contains elements of each lobe sub-environment; however, there is an increasing prevalence of higher-density deposits upwards through stratigraphy. This pattern is interpreted as representing overall lobe progradation. Colored bars next to logs represent facies on sub-environment key.

Fig. 10 A) Medium-density turbidite (MDT) at Col du Fa. **B)** Low-density turbidite **(**LDT) onlapping a gravel lag deposit at Tête du Ruch (Lower). **C)** Organic material in the debritic division of a hybrid bed at Le Marc. **D)** Pinch-out amalgamation zone at Col du Fa. Debritic (Db) and turbiditic (Tb) sections can be identified and correlate with thick- and medium-bedded turbidites up-dip. It is difficult to differentiate groups of event-beds in these slope proximal units. **E)** Highly tractionally r-worked LDT. **F)** Typical thin-bedded LDT facies. **G)** Slumped thin-bedded turbidites at Argenton. Fold hinges indicate failure perpendicular to the slope.

Fig. 11: A) Contact between the thin beds and high-density turbidites at Col du Fa. The high-density turbidites onlap against the low-density turbidite slope drape at an incidence angle almost perpendicular to the slope (arrow is paleoflow). **B)** Example of a high-density turbidite with a wedged base onlapping the underlying slope drape. Restoring the bed top to horizontal allows a rough estimate of the paleo-slope angle. **C)** Scar fill at Tête de Ruch (upper). The higher-density flows either onlap the scar drape abruptly or transform to low-density turbidites up the counter-slope. **D)** Laterally continuous hybrid beds at Le Marc. These beds are interpreted to have been deposited away from the basin margin and cohesively transformed through distal run-out. 7 cm camera lens (black circle) for scale.

Fig. 12: High-resolution log of one medium-density turbidite approaching onlap at Col du Fa showing the short length-scale variability seen in these beds.

Fig. 13: A) Hybrid-bed evolution approaching topography at Argenton. **B)** Hybrid evolution at Tête de Ruch (lower**) C)** Hybrid-bed evolution at the Tête de Ruch (upper). The complex interaction between the debritic and turbiditic intervals are suggested to result from either differential interaction with the slope between rheologically distinct flow phases or erosion at the onlap surface. Letters in blacked boxes = correlated bed label. Log key on Fig. 6.

Fig. 14: Outcrop sketch from the Col du Fa locality. **A)** Low-density turbidites drape the slope and are onlapped by hybrid beds and higher-density turbidites. **B)** Flow transformation can be seen to occur in the proximal fringe deposits over 10 - 15 m approaching the onlap surface to the NW, resulting in complex amalgamation zones at pinch-out (see Fig. 10D for pinch-out detail).

Fig. 15: Example of correlated low-density turbidites approaching the Col du Fa basin margin. Very little facies variation is seen in these beds and thinning rates are lower than those seen within thicker-bedded turbidites approaching the basin margin.

Fig. 16: Summary logs showing facies transition approaching pinch-out toward basin margins for given lobe sub-environments and their dominant facies. The right-hand petrographic images are taken from representative beds in the Annot Basin approaching onlap. The corresponding letter (white text in black box) on the logs indicates the point in the bed where the sample was taken. Onlap to right.

Fig. 17: Synthesis of facies evolutions seen in the Grès d'Annot towards the basin margins and their stratigraphic position. Flow concentration at the point of sedimentation largely controls the style of the onlap termination. Lobe sub-environments are often obscured adjacent to onlap surfaces due to topographic interaction between the flow and the slope, but can be back-stripped.

Fig. 18: A) Run-up height versus flow sediment concentration for flows of varying velocities. Flows with high concentrations are less able to run up topography than low-concentration flows if all other parameters are equal. **B)** Run-up height versus the angle of incidence between the flow and the slope for flows of varying velocities. Lower angles of incidence cause higher run-up of flows. **C)** Schematic diagram showing the relationship between frontal and lateral onlap (modified from Al A'Jaidi et al. 2004).

Fig. 19: Model for the stratigraphic evolution of flow terminations in a static confined deep-water basin. It is suggested that the pattern of termination trends may be used to predict the termination style expected at a given point on the onlap surface. Flow transformation, which increases flow concentration, results can result in offlap. Similarly, bypass of the upper parts of axial flows results in offlap of the deposits of the highly concentrated basal layers of these flows against the underlying deposits. Concurrent hemipelagic deposition has been ignored for simplicity.

Fig. 20: Model for the progradation of a clastic system into an intra-slope minibasin. Representative logs (A, B, and C) of the various sub-environments are indicated.

Fig. 21: Types of intra-formational onlap that can be recognized in confined deep-water basins (modified from Sinclair and Tomasso, 2002). A distinction is made between autogenic onlap, caused by longitudinal flow evolution over shorter timescales, and allogenic onlap, caused by tectonic subsidence over longer timescales. Autogenic processes will create short-length-scale heterogeneities in larger-scale and allogenically controlled sequences.

Table 1: Key lithofacies, facies associations, and onlap geometries seen in the Grès d'Annot of the Annot Basin.

1164

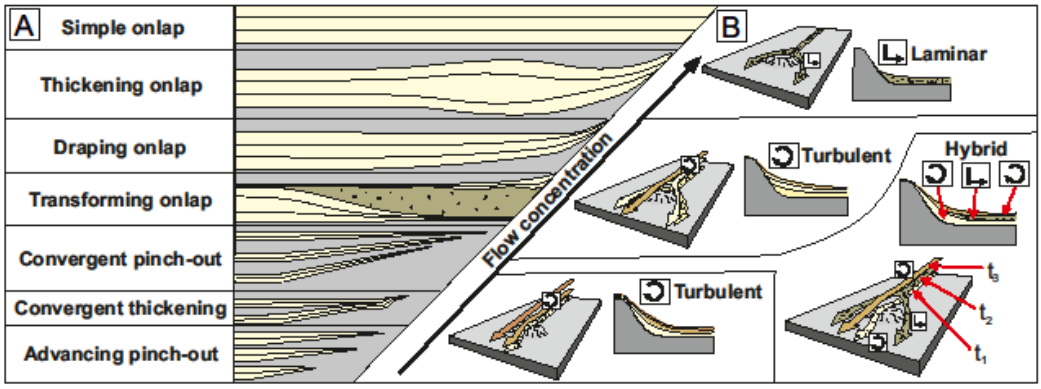

1165
1166

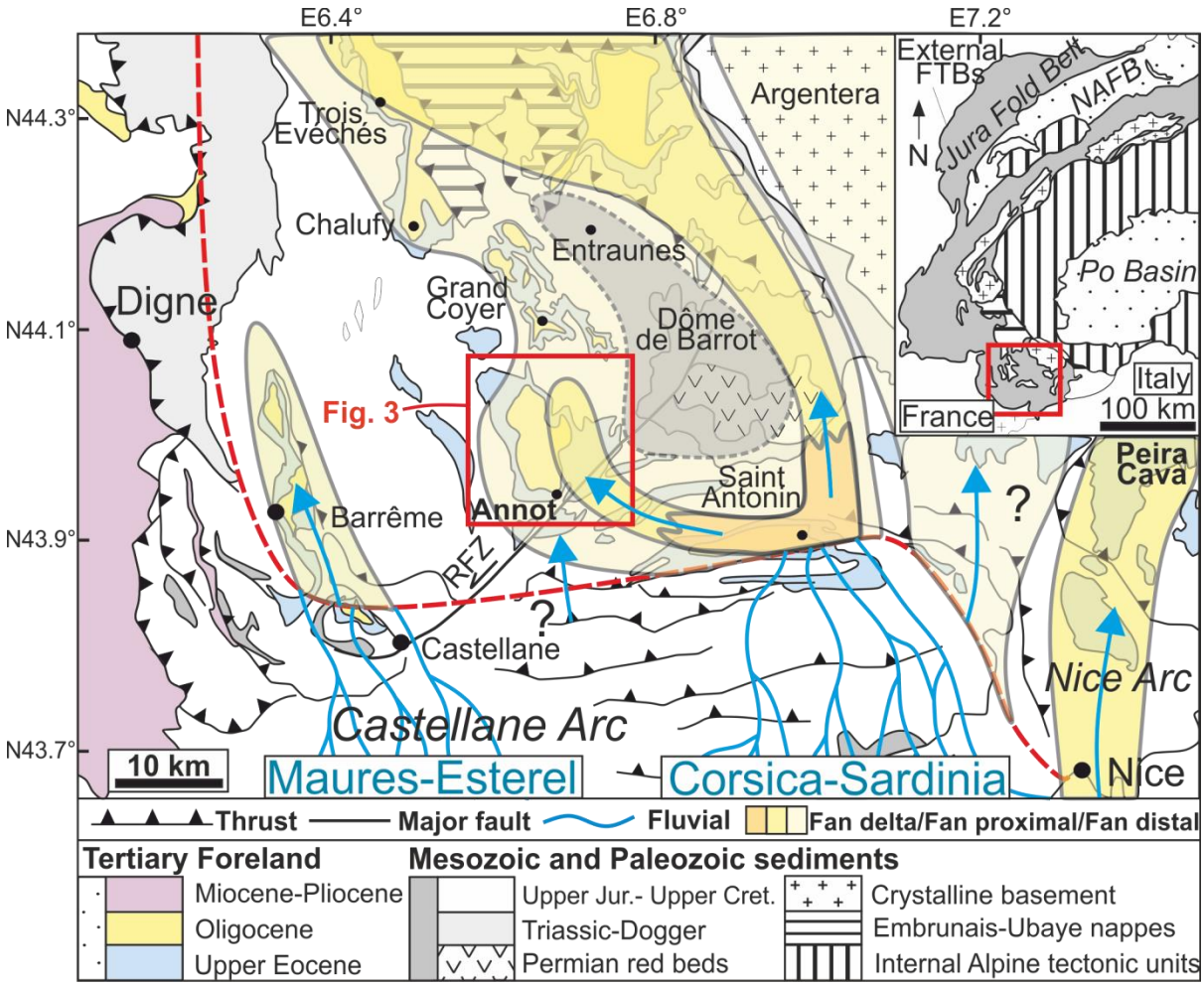
E6.4°
E6.8°
E7.2°
N44.3°
N44.1°
N43.9°
N43.7°
Trois Evêchés
Chalufy
Entraunes
Argentera
Grand Coyer
Dôme de Barrot
Digne
Fig. 3
Barrême
Annot
Saint Antonin
RFZ
?
Castellane
Castellane Arc
Maures-Esterel
Corsica-Sardinia
Nice Arc
Nice
Peira Cava
10 km
External FTBs
N
Jura Fold Belt
NAFB
Po Basin
Italy
France
100 km
Thrust
Major fault
Fluvial
Fan delta/Fan proximal/Fan distal
Tertiary Foreland
Miocene-Pliocene
Oligocene
Upper Eocene
Mesozoic and Paleozoic sediments
Upper Jur.- Upper Cret.
Triassic-Dogger
Permian red beds
Crystalline basement
Embrunais-Ubaye nappes
Internal Alpine tectonic units

1167

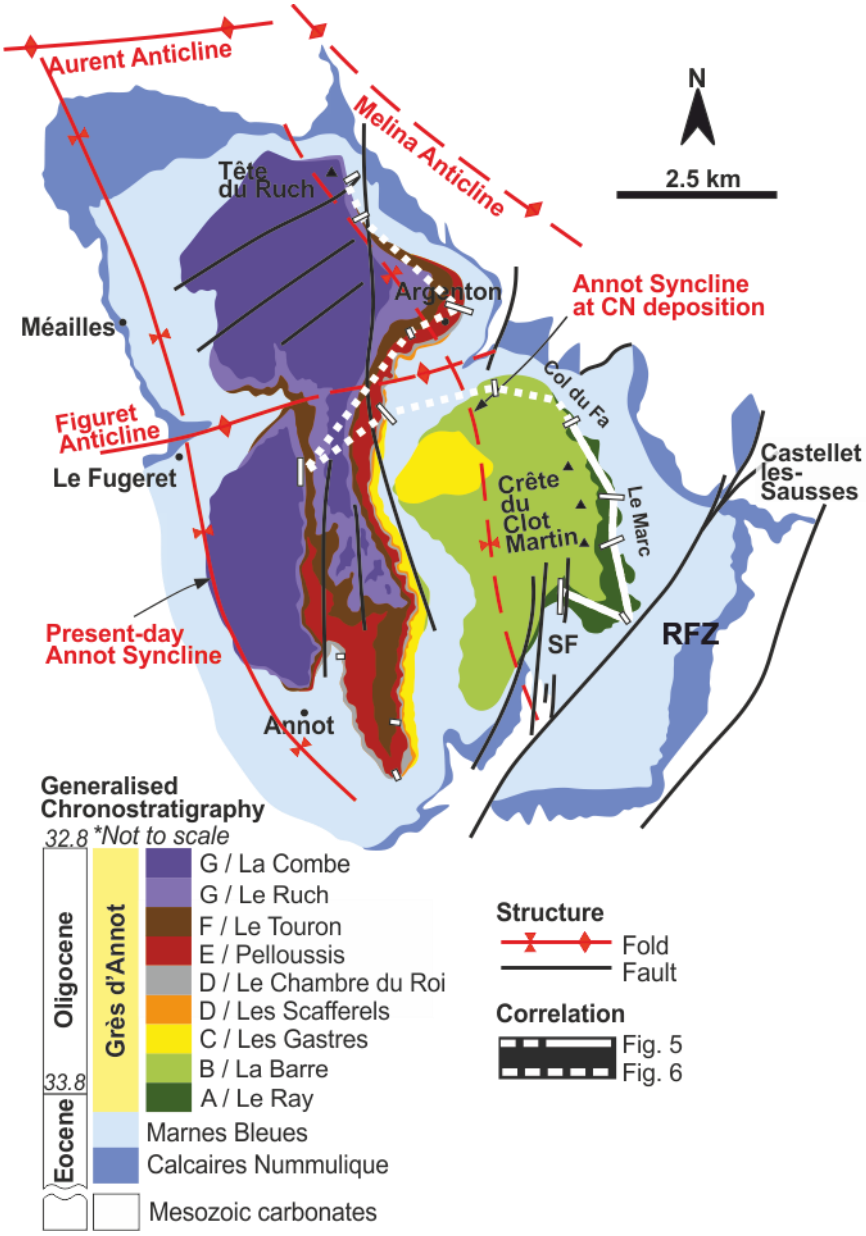
Aurent Anticline
Melina Anticline
N
2.5 km
Tête du Ruch
Argenton
Annot Syncline at CN deposition
Méailles
Col du Fa
Figuret Anticline
Le Fugeret
Crête du Clot Martin
Le Marc
Castellet les-Sausses
Present-day Annot Syncline
SF
RFZ
Annot
Generalised Chronostratigraphy
*Not to scale
32.8
33.8
Oligocene
Eocene
Grès d'Annot
G / La Combe
G / Le Ruch
F / Le Touron
E / Pelloussis
D / Le Chambre du Roi
D / Les Scafferels
C / Les Gastres
B / La Barre
A / Le Ray
Marnes Bleues
Calcaires Nummulique
Mesozoic carbonates
Structure
Fold
Fault
Correlation
Fig. 5
Fig. 6

1168

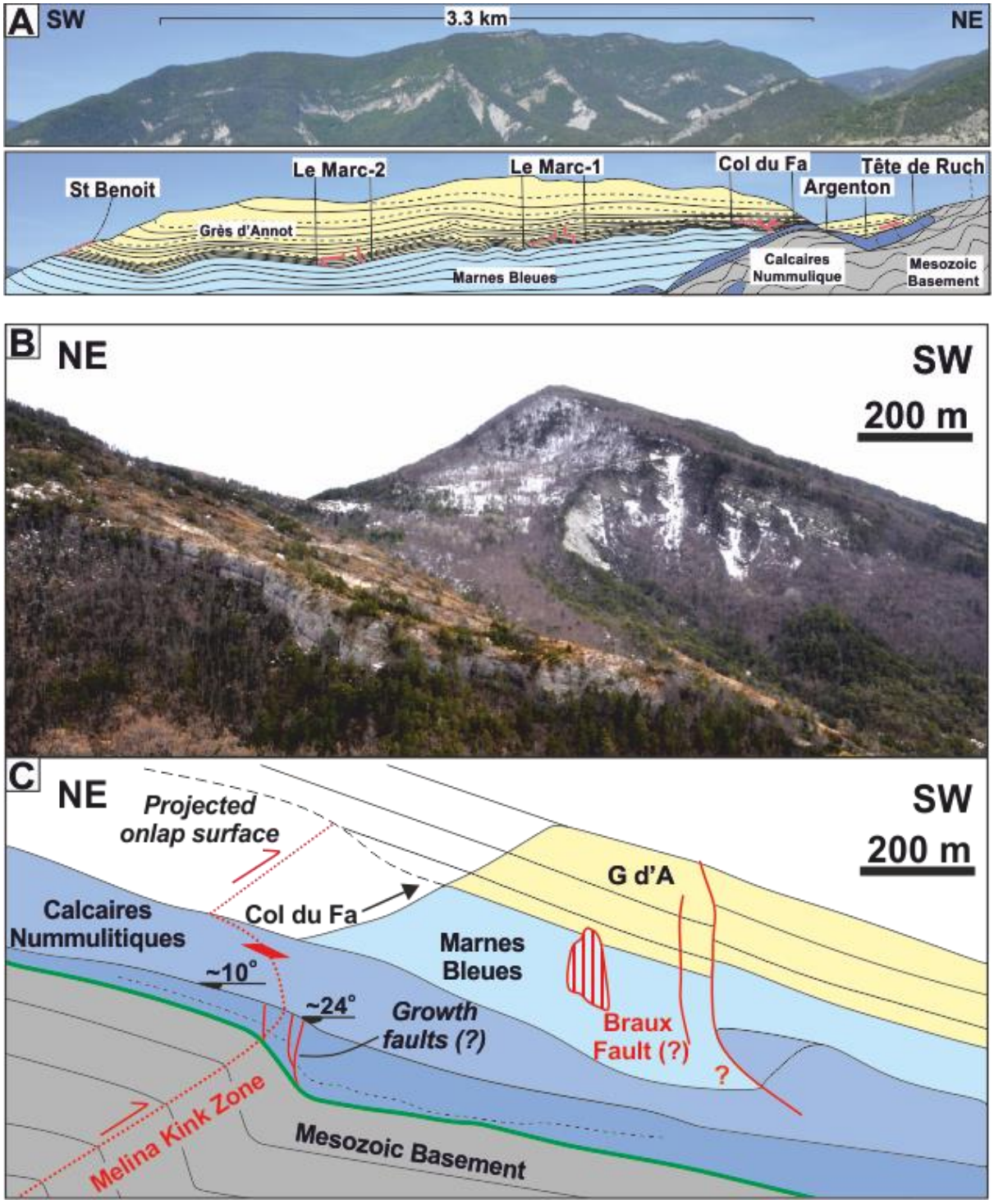
A
SW
3.3 km
NE
St Benoit
Le Marc-2
Le Marc-1
Col du Fa
Argenton
Tête de Ruch
Grès d'Annot
Marnes Bleues
Calcaires Nummulique
Mesozoic Basement
B
NE
SW
200 m
C
NE
SW
200 m
Projected onlap surface
Col du Fa
G d'A
Calcaires Nummulitiques
Marnes Bleues
~10°
~24°
Growth faults (?)
Braux Fault (?)
?
Melina Kink Zone
Mesozoic Basement

1169
1170

1171

1172 =

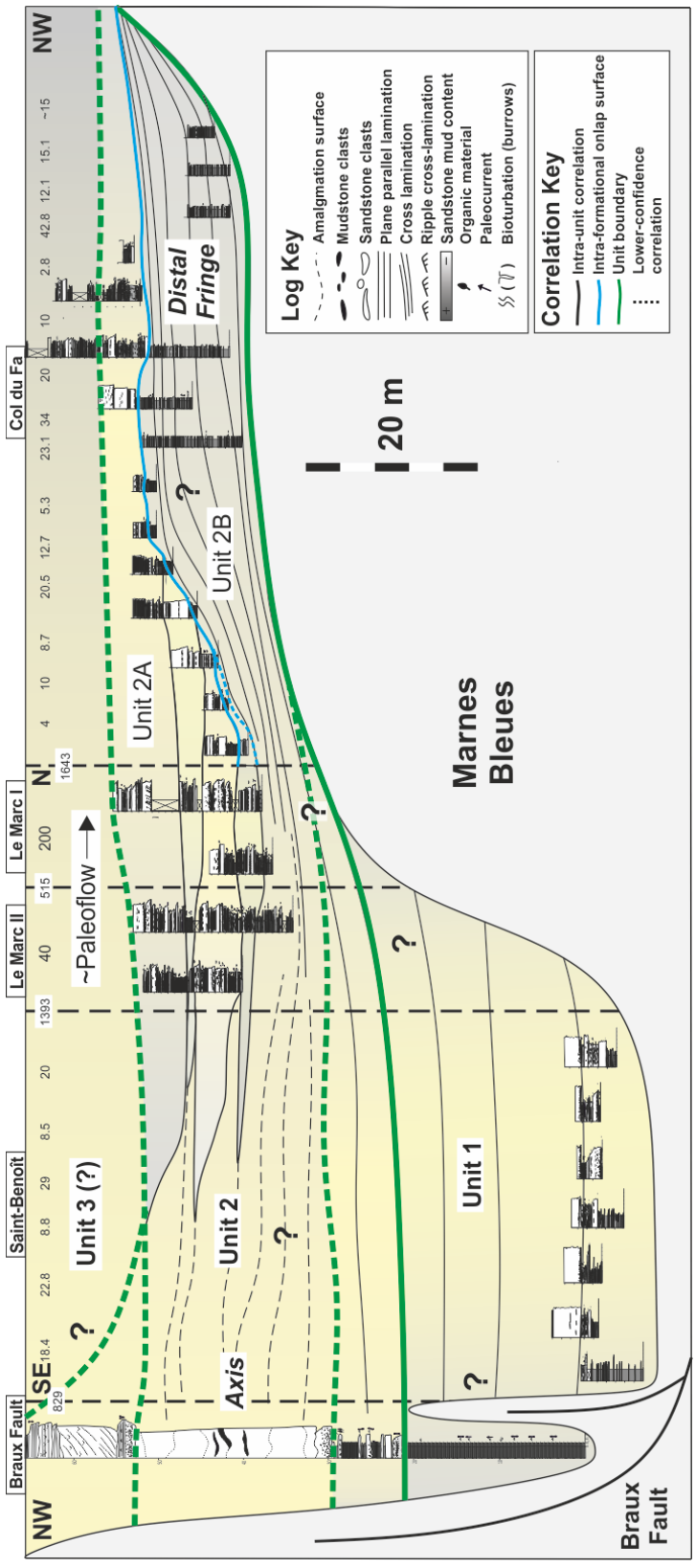

1173

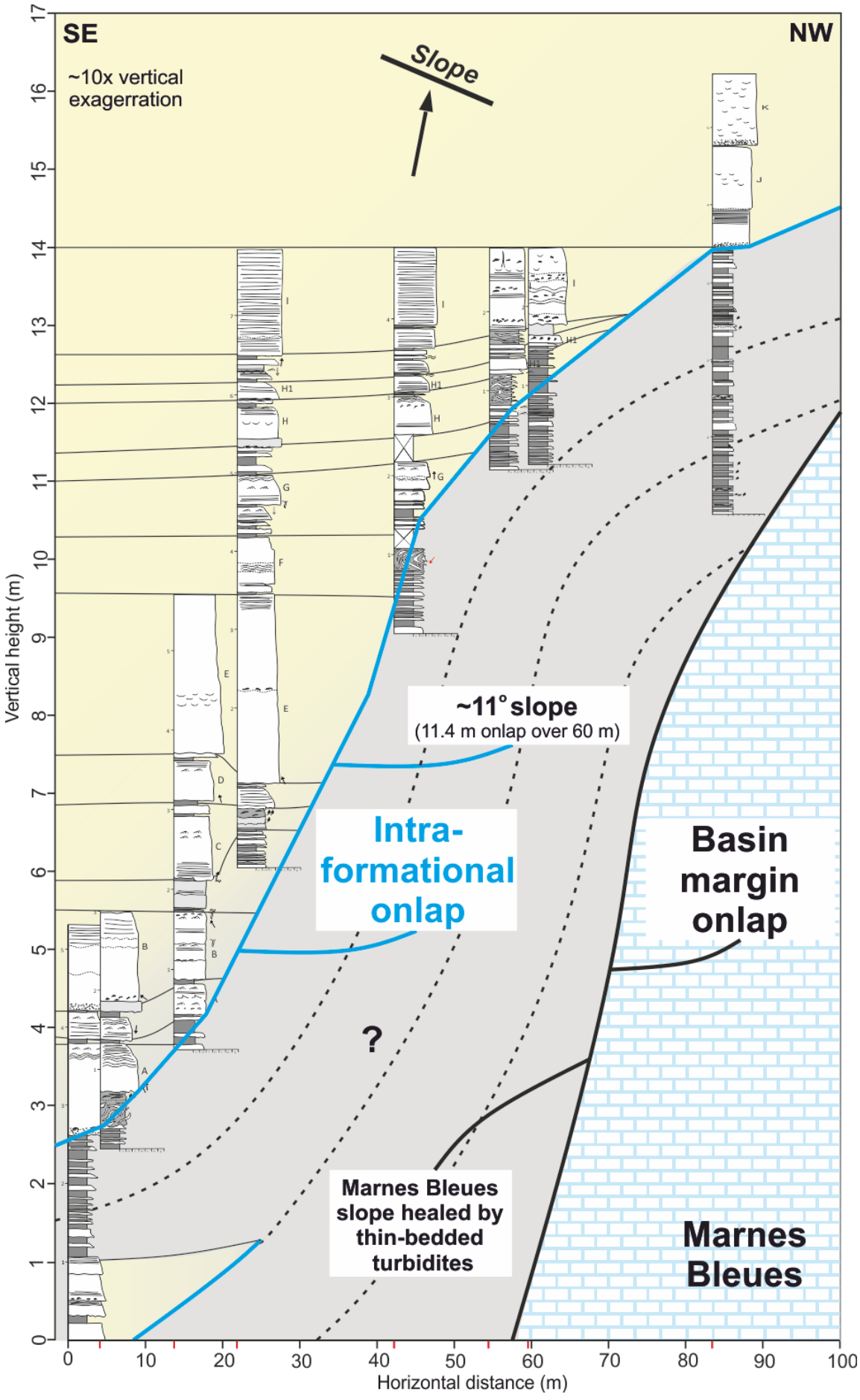
SE
NW
~10x vertical exagerration
Slope
~11° slope
(11.4 m onlap over 60 m)
Intra-formational onlap
Basin margin onlap
?
Marnes Bleues slope healed by thin-bedded turbidites
Marnes Bleues
Vertical height (m)
Horizontal distance (m)

1174

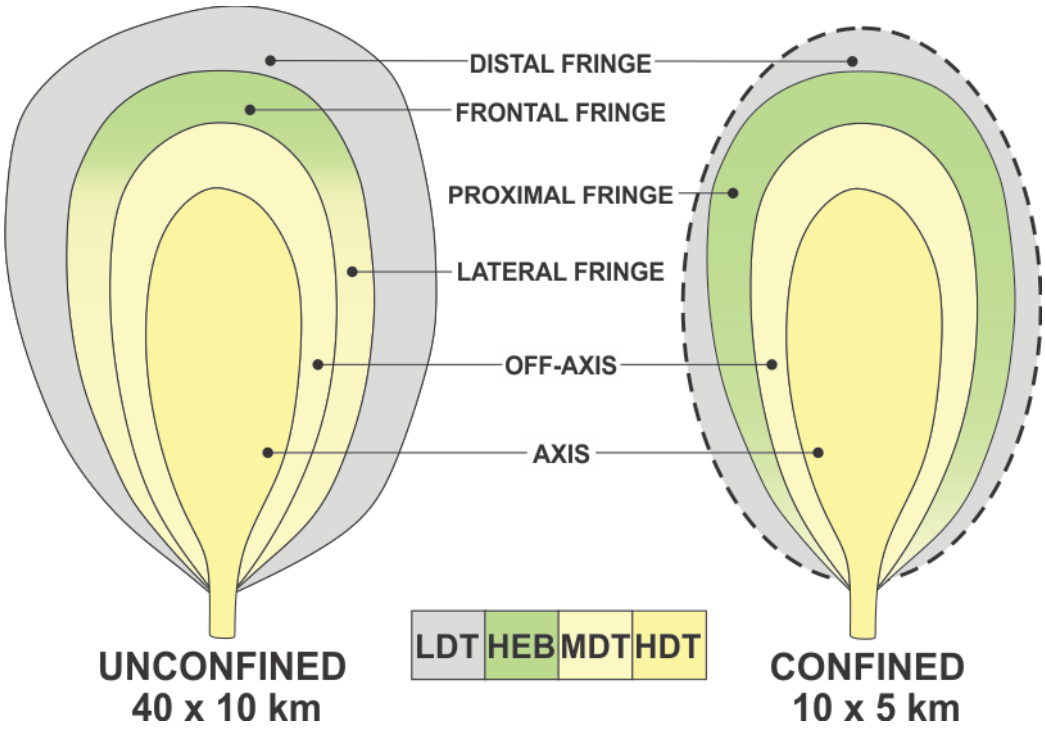
DISTAL FRINGE
FRONTAL FRINGE
PROXIMAL FRINGE
LATERAL FRINGE
OFF-AXIS
AXIS
LDT
HEB
MDT
HDT
UNCONFINED
40 x 10 km
CONFINED
10 x 5 km

1175

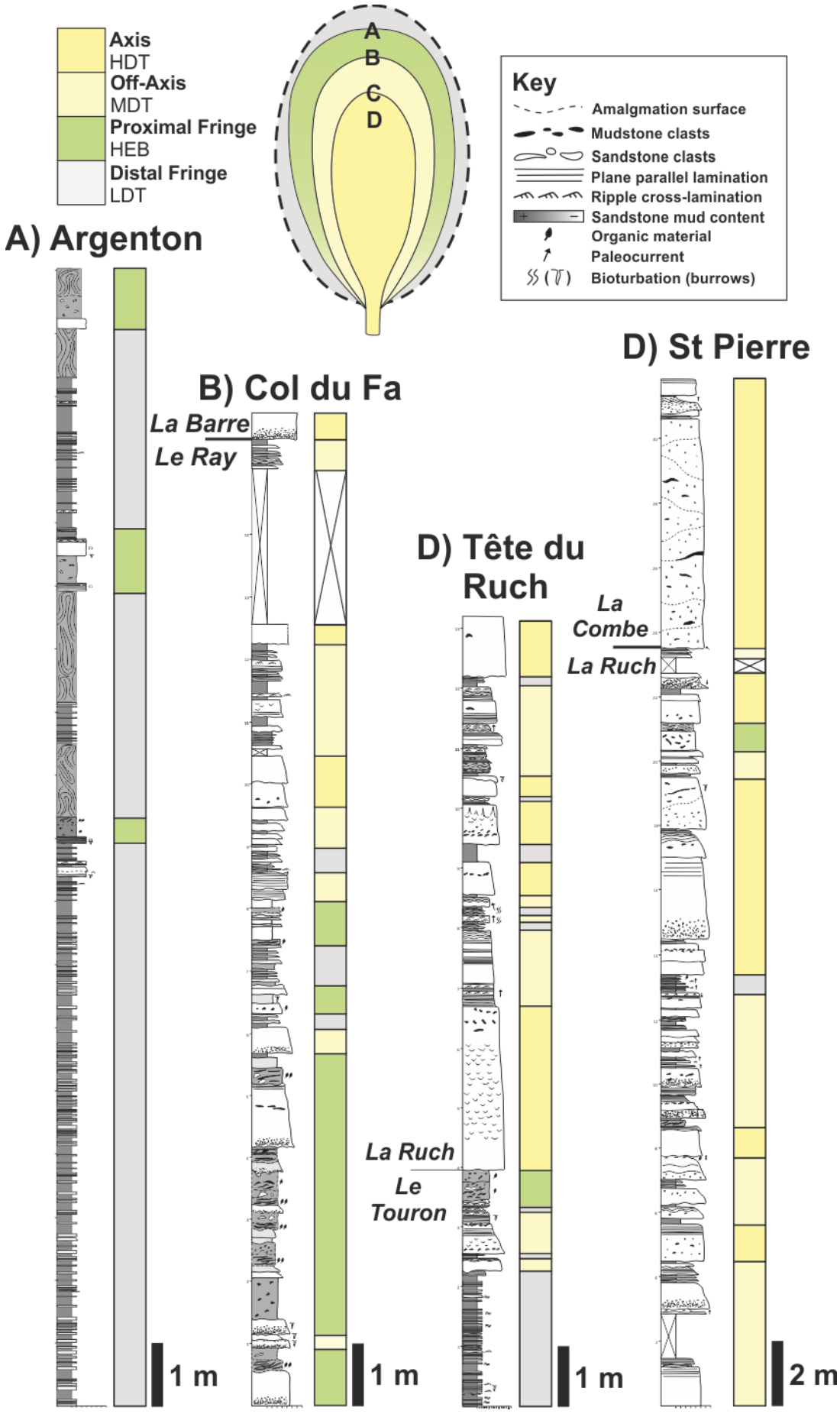
Axis
HDT
Off-Axis
MDT
Proximal Fringe
HEB
Distal Fringe
LDT
A
B
C
D
Key
Amalgmation surface
Mudstone clasts
Sandstone clasts
Plane parallel lamination
Ripple cross-lamination
Sandstone mud content
Organic material
Paleocurrent
Bioturbation (burrows)
A) Argenton
B) Col du Fa
La Barre
Le Ray
D) Tête du Ruch
La Ruch
Le Touron
D) St Pierre
La Combe
La Ruch
1 m
1 m
1 m
2 m

1176

1177

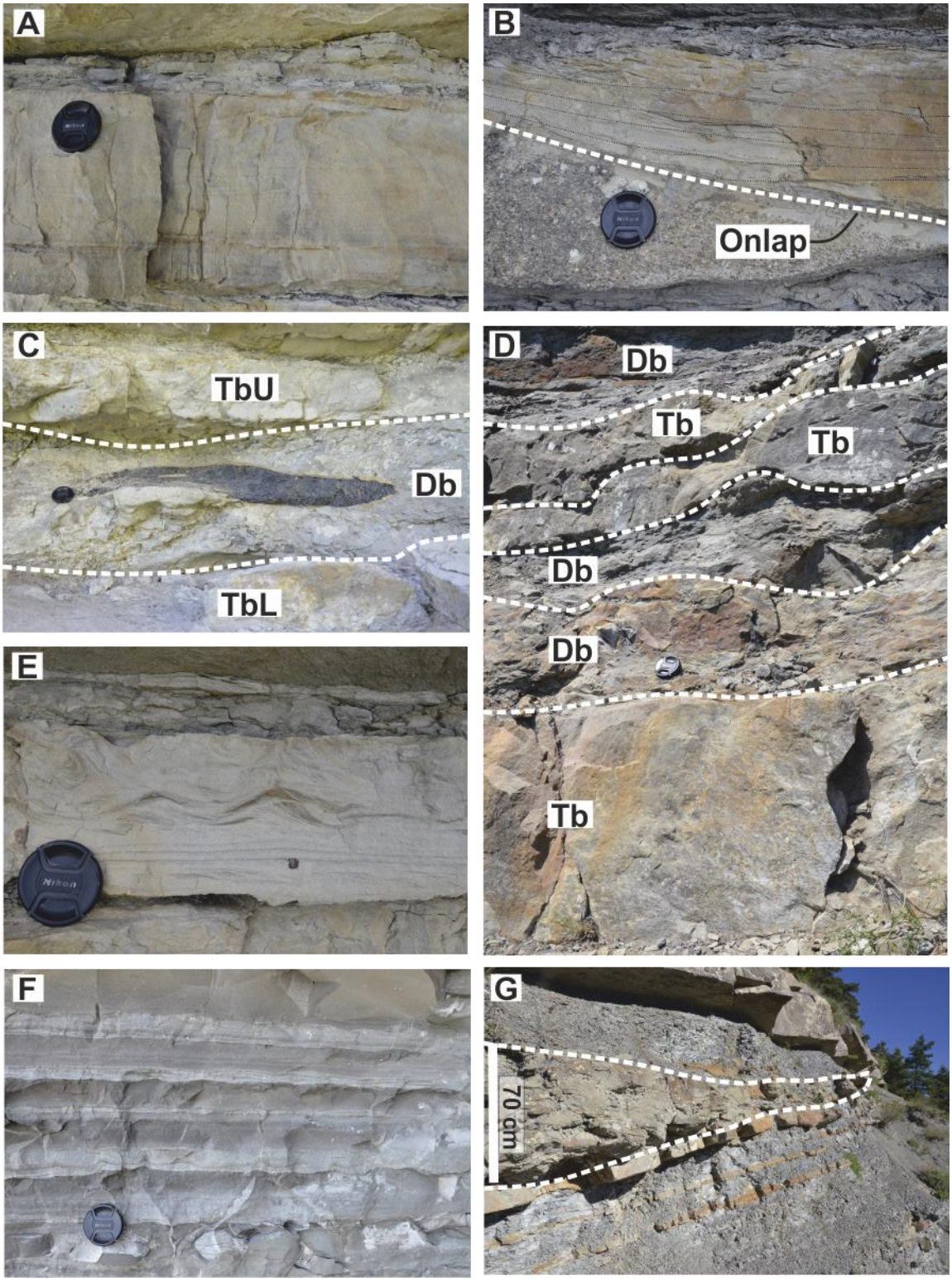

1178

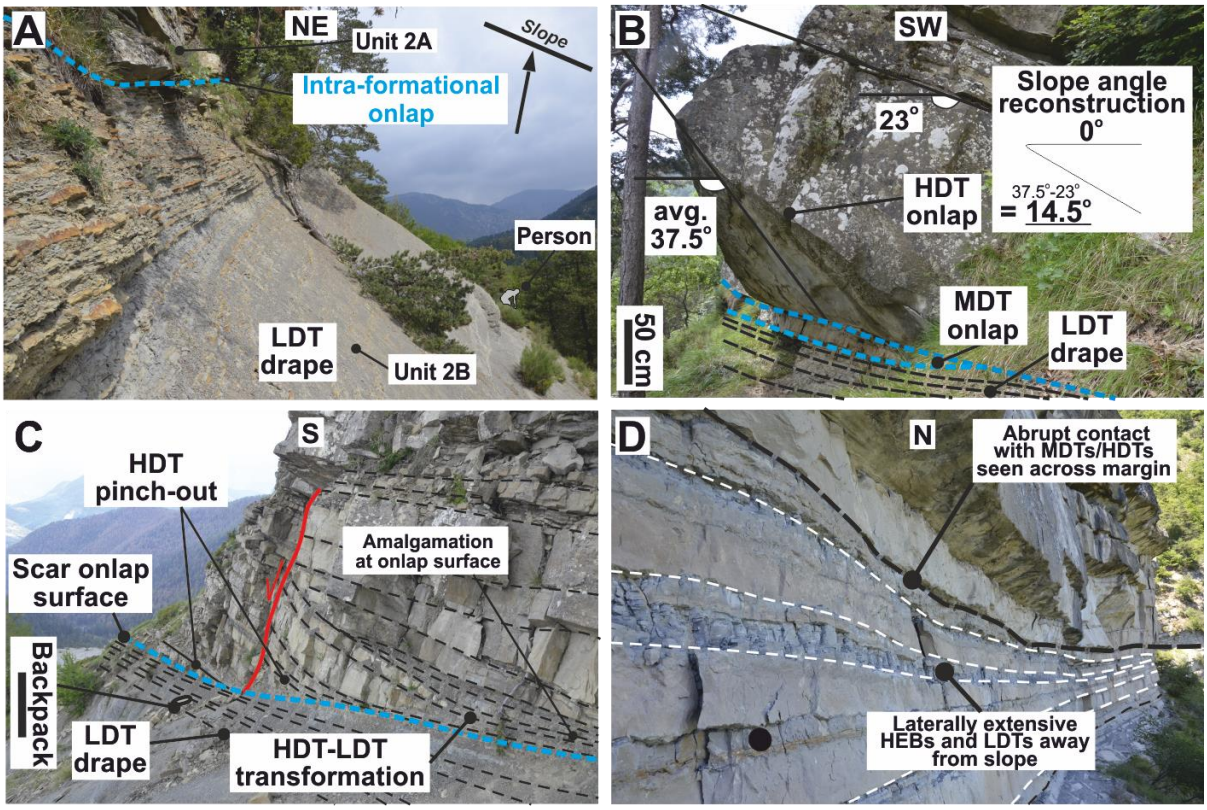
A
NE
Unit 2A
Slope
Intra-formational onlap
Person
LDT drape
Unit 2B
B
SW
Slope angle reconstruction
0°
23°
HDT onlap
37.5°-23°
= 14.5°
avg. 37.5°
50 cm
MDT onlap
LDT drape
C
S
HDT pinch-out
Amalgamation at onlap surface
Scar onlap surface
Backpack
LDT drape
HDT-LDT transformation
D
N
Abrupt contact with MDTs/HDTs seen across margin
Laterally extensive HEBs and LDTs away from slope

1179

1180

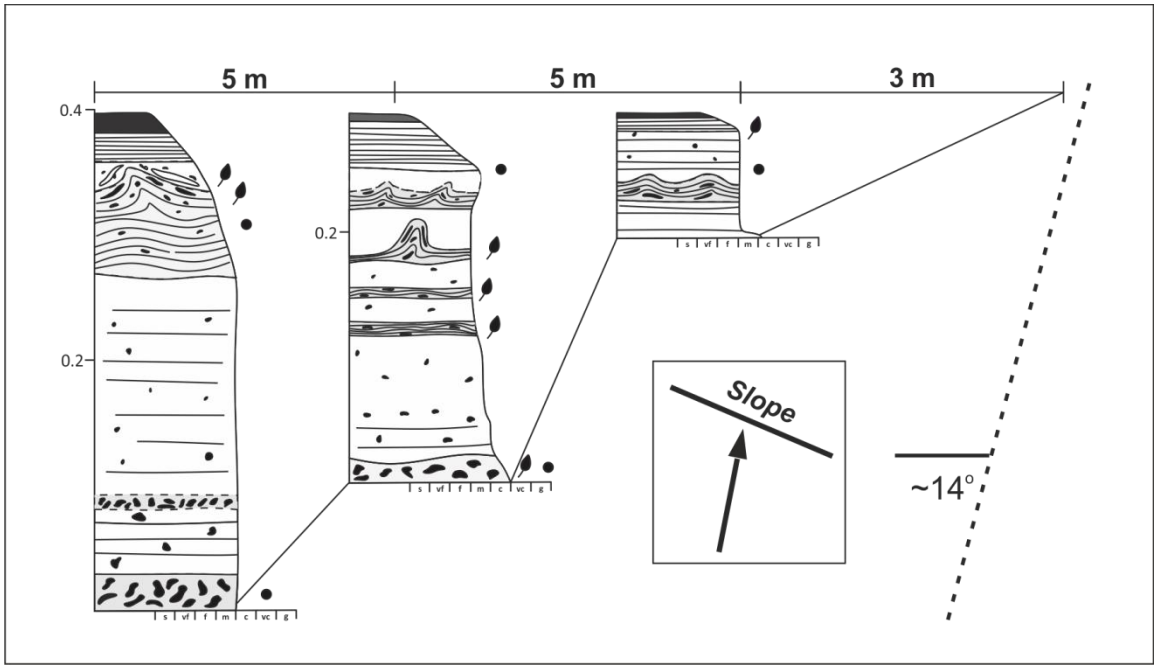

1181

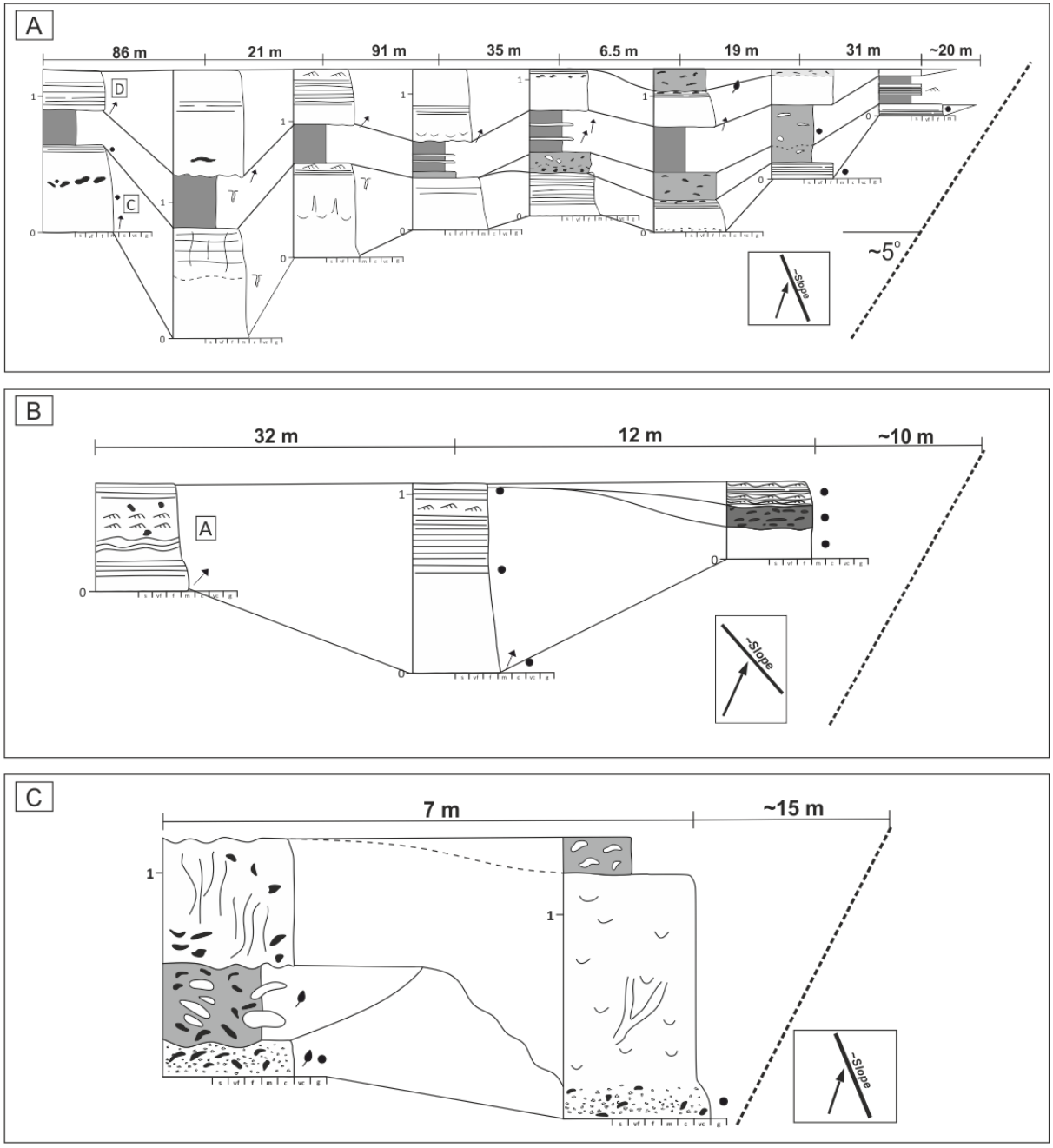
A
86 m
21 m
91 m
35 m
6.5 m
19 m
31 m
~20 m
D
C
~5°
~Slope
B
32 m
12 m
~10 m
A
~Slope
C
7 m
~15 m
~Slope

1182

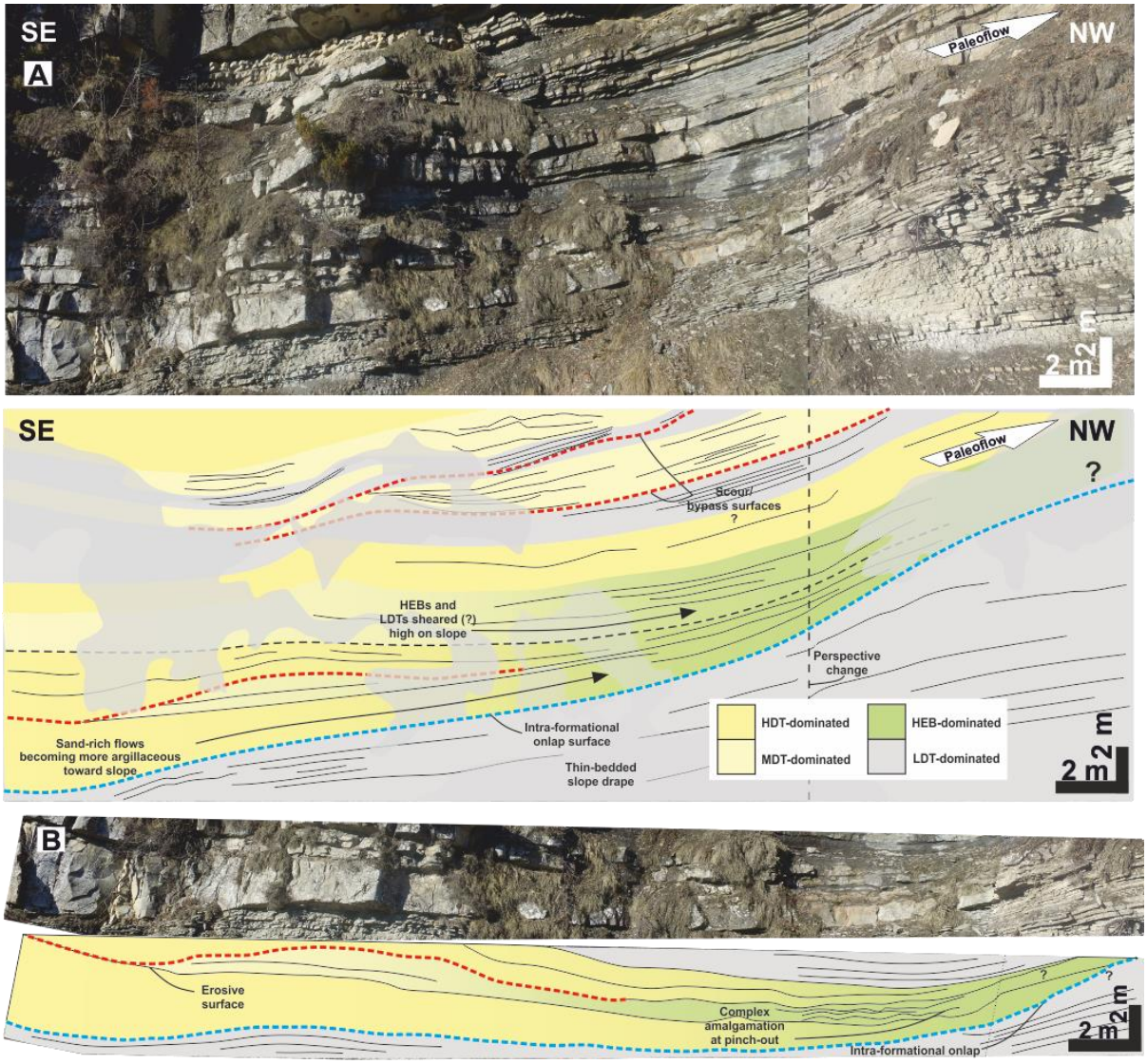
SE
A
Paleoflow
NW
2 m
SE
NW
Paleoflow
?
Scour/
bypass surfaces
?
HEBs and
LDTs sheared (?)
high on slope
Perspective
change
Intra-formational
onlap surface
Sand-rich flows
becoming more argillaceous
toward slope
Thin-bedded
slope drape
HDT-dominated
MDT-dominated
HEB-dominated
LDT-dominated
2 m
B
Erosive
surface
Complex
amalgamation
at pinch-out
Intra-formational onlap
2 m

1183

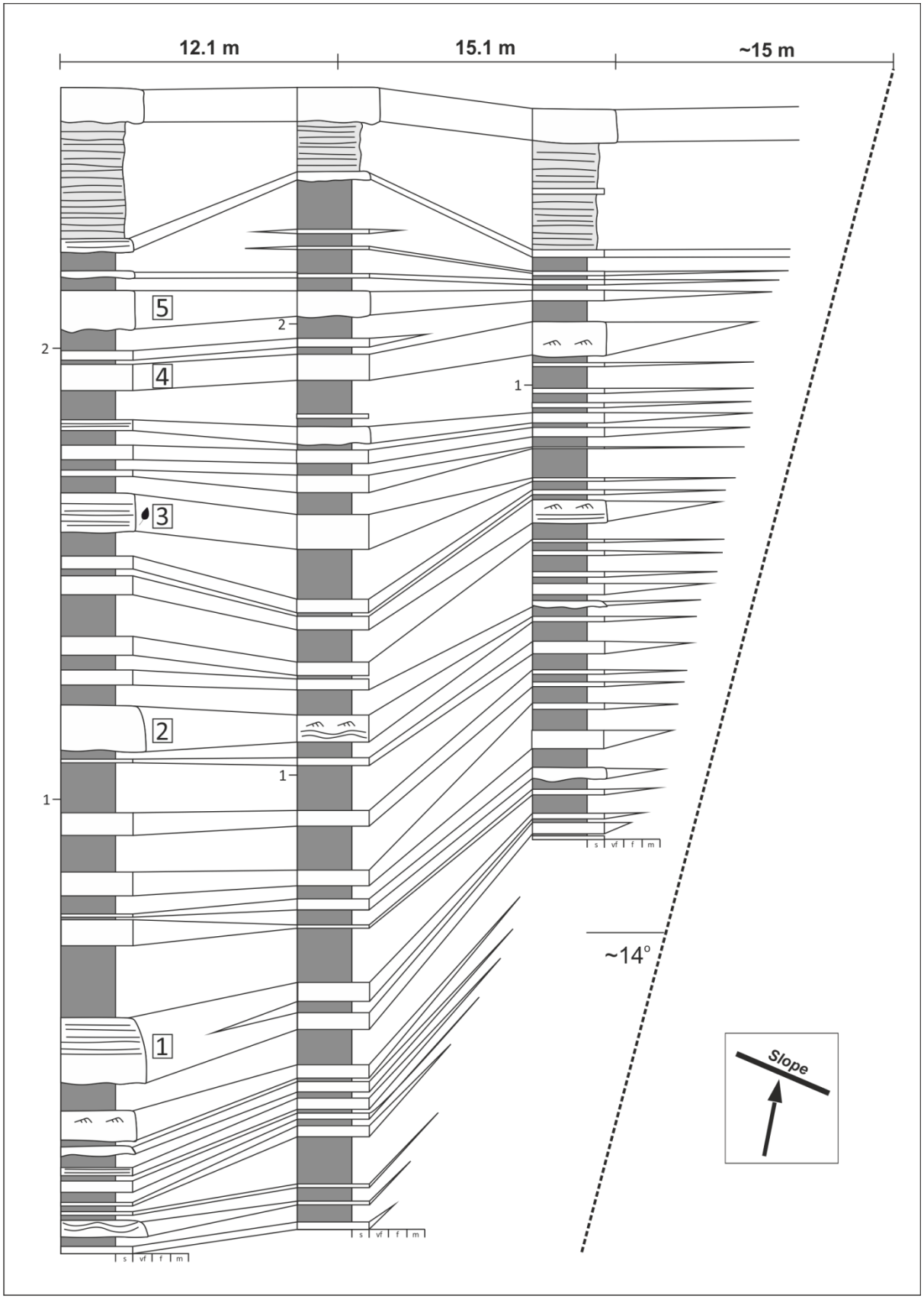

1184

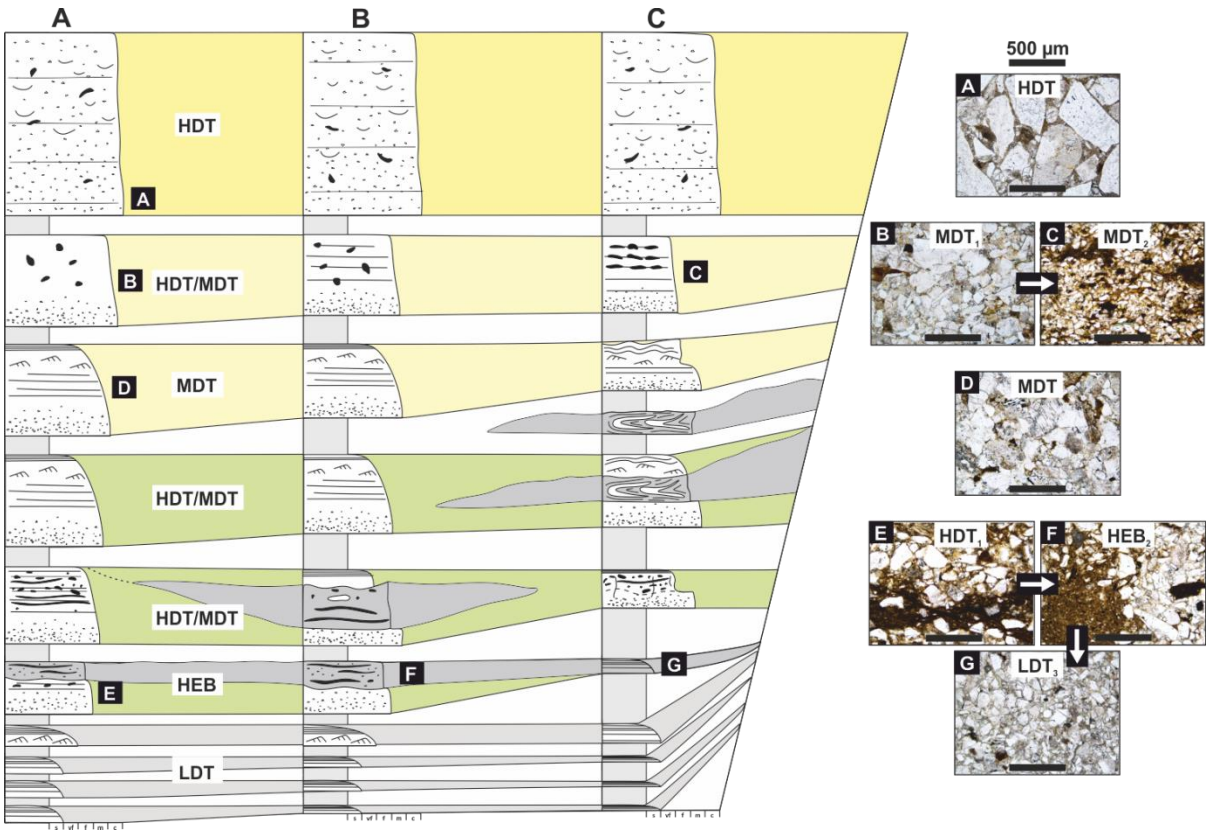
A
B
C
HDT
A
B
HDT/MDT
C
D
MDT
HDT/MDT
HDT/MDT
E
HEB
F
G
LDT
500 µm
A
HDT
B
MDT1
C
MDT2
D
MDT
E
HDT1
F
HEB2
G
LDT3

1185

1186

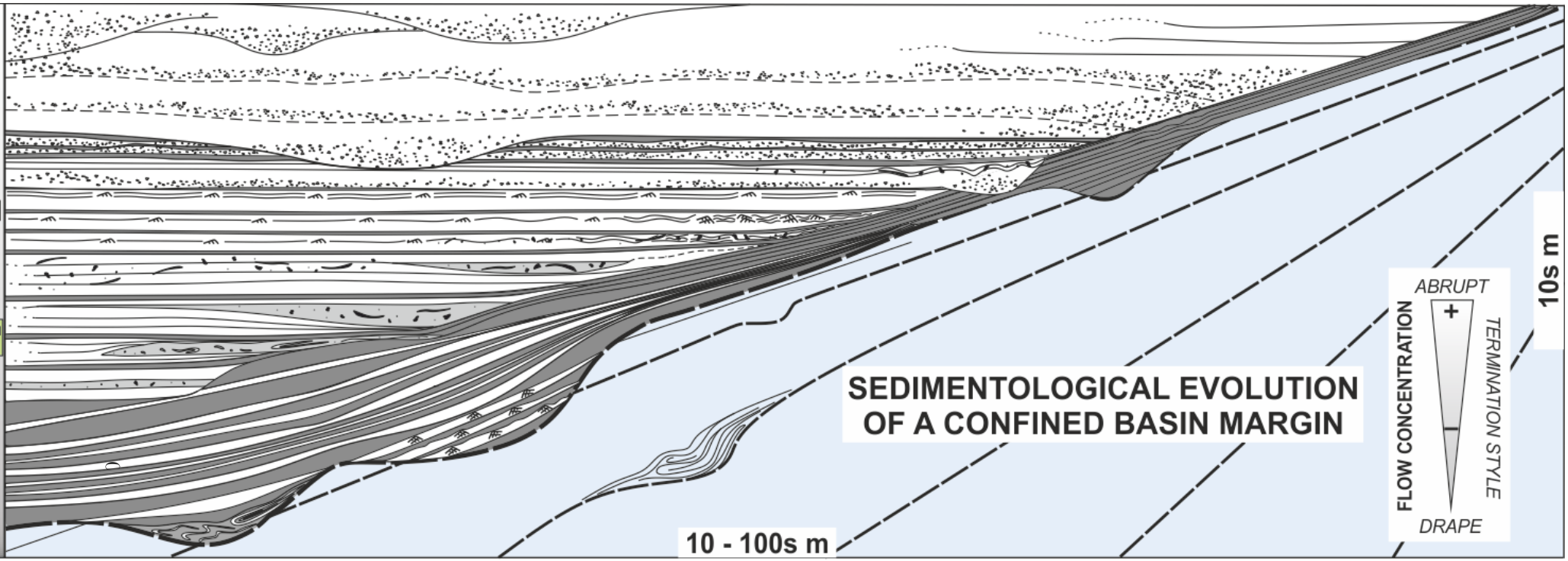
SEDIMENTOLOGICAL EVOLUTION
OF A CONFINED BASIN MARGIN
10 - 100s m
10s m
ABRUPT
+
–
DRAPE
FLOW CONCENTRATION
TERMINATION STYLE

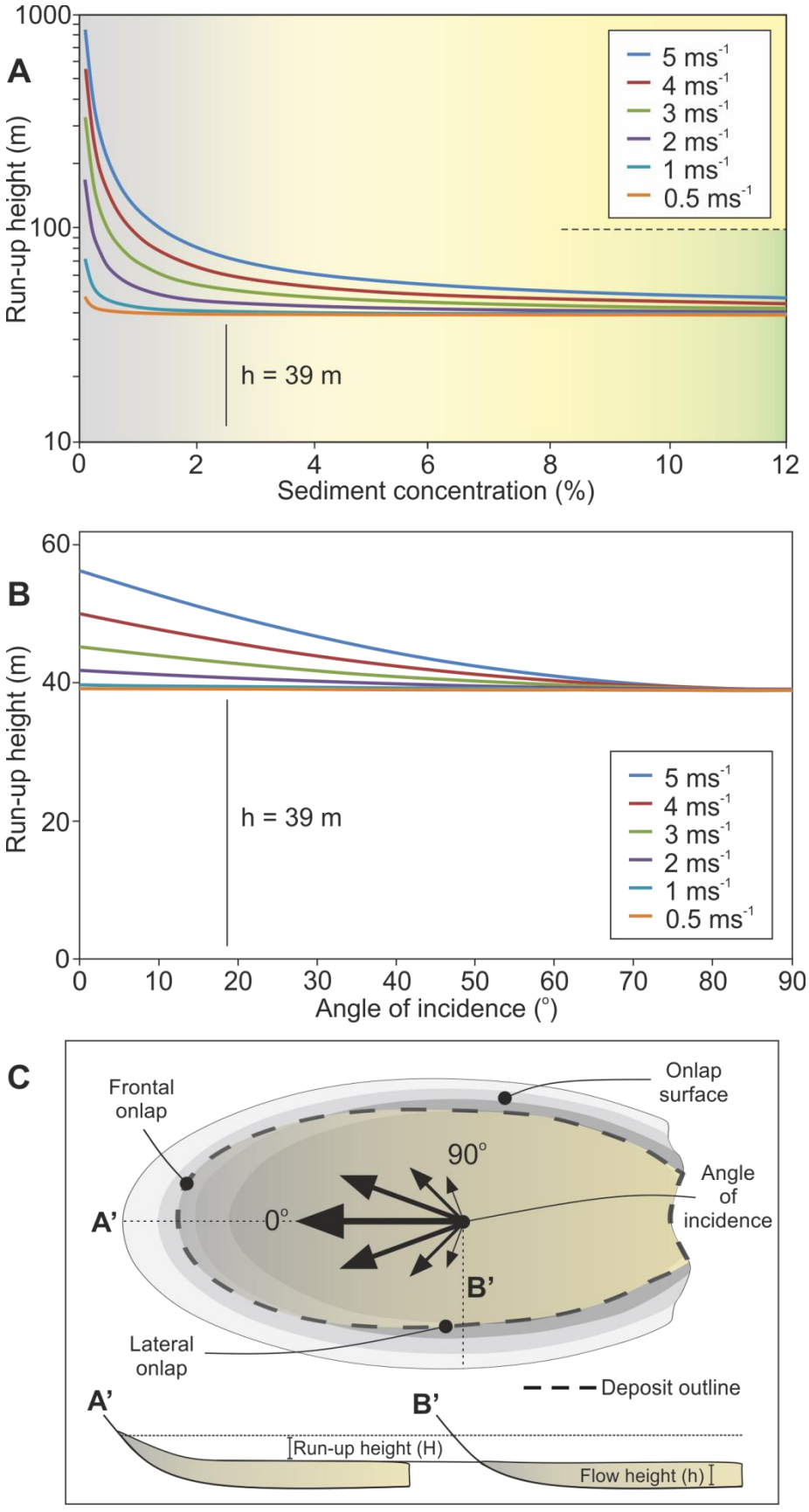
A
Run-up height (m)
1000
100
10
0
2
4
6
8
10
12
Sediment concentration (%)
5 ms-1
4 ms-1
3 ms-1
2 ms-1
1 ms-1
0.5 ms-1
h = 39 m
B
Run-up height (m)
60
40
20
0
0
10
20
30
40
50
60
70
80
90
Angle of incidence (°)
5 ms-1
4 ms-1
3 ms-1
2 ms-1
1 ms-1
0.5 ms-1
h = 39 m
C
Frontal onlap
Onlap surface
90°
Angle of incidence
A'
0°
B'
Lateral onlap
Deposit outline
A'
B'
Run-up height (H)
Flow height (h)

1188

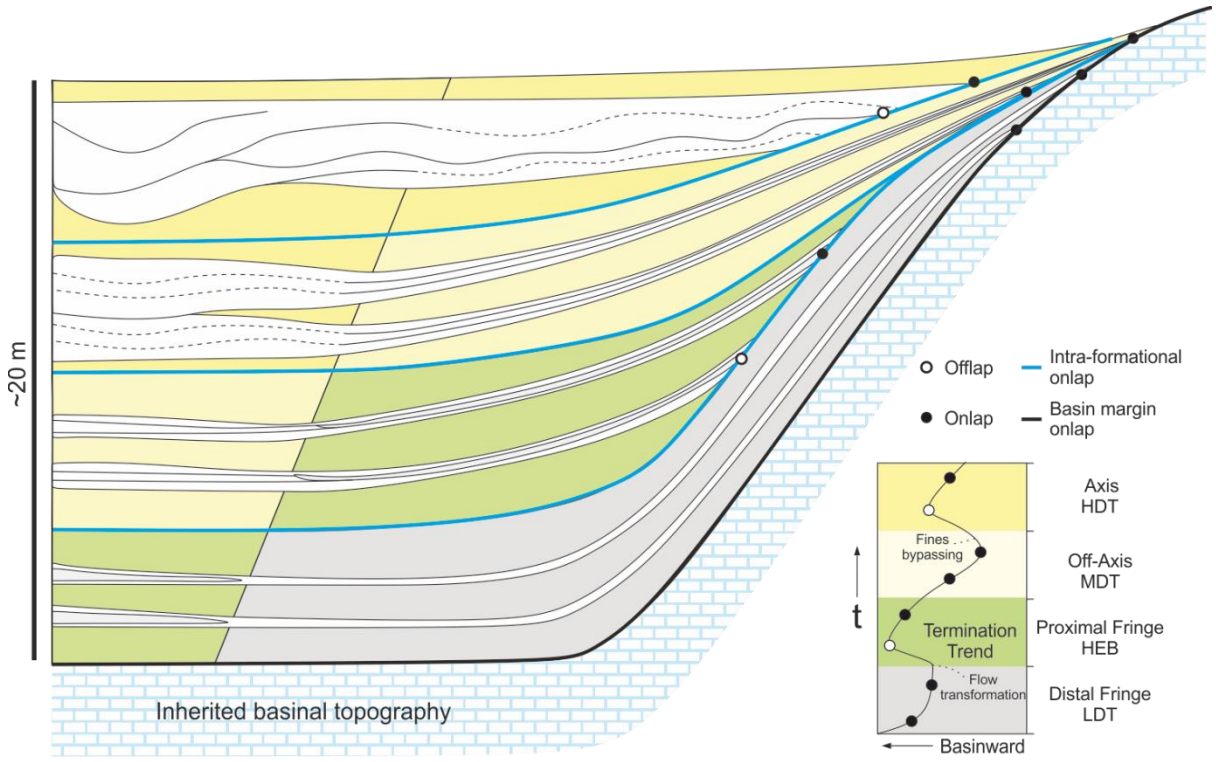
~20 m
Inherited basinal topography
Offlap
Onlap
Intra-formational onlap
Basin margin onlap
Axis
HDT
Fines bypassing
Off-Axis
MDT
t
Termination Trend
Proximal Fringe
HEB
Flow transformation
Distal Fringe
LDT
Basinward

1189

1190

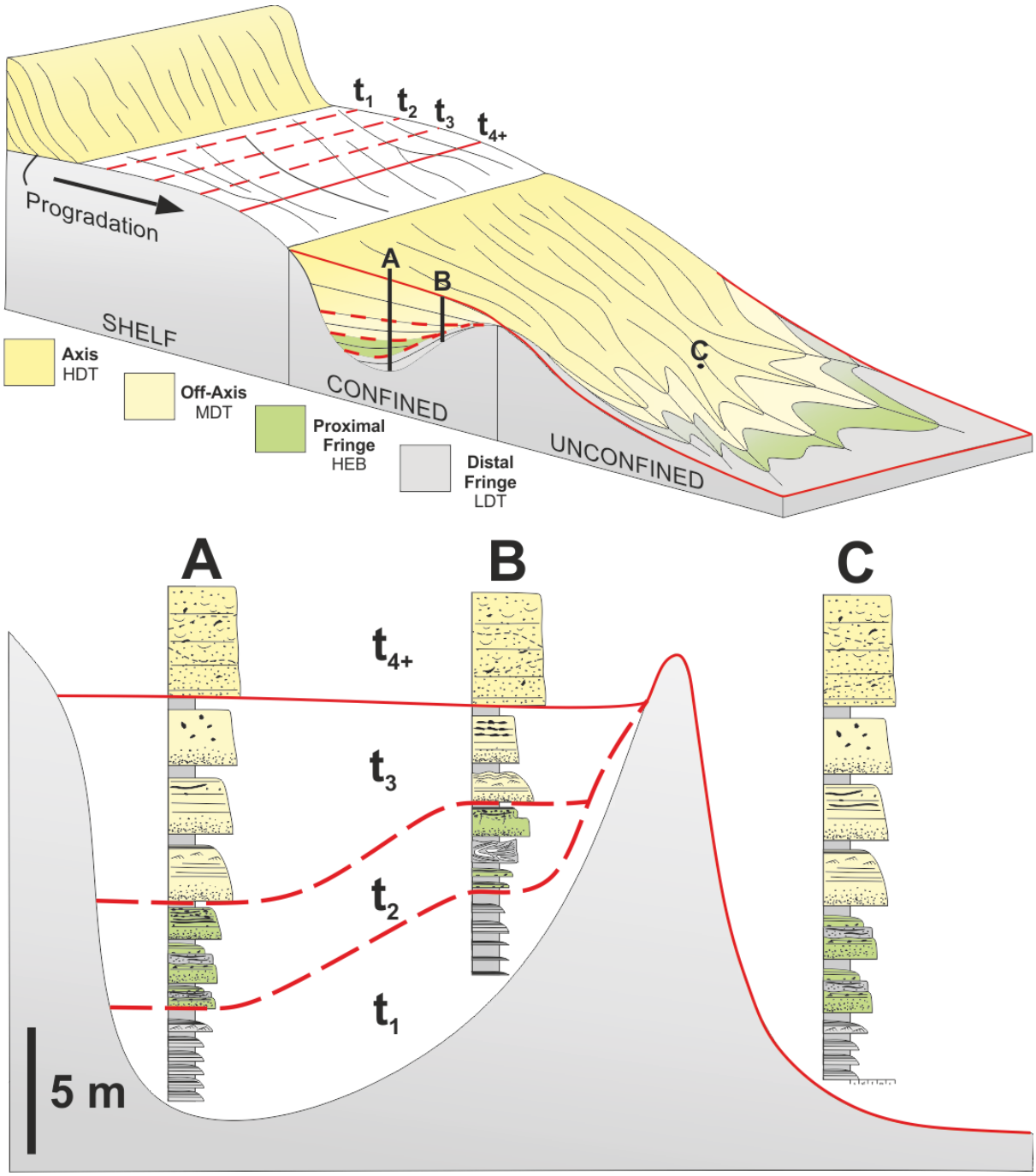
t1 t2 t3 t4+
Progradation
A
B
C
SHELF
CONFINED
UNCONFINED
Axis
HDT
Off-Axis
MDT
Proximal
Fringe
HEB
Distal
Fringe
LDT
A
B
C
t4+
t3
t2
t1
5 m

1191

1192

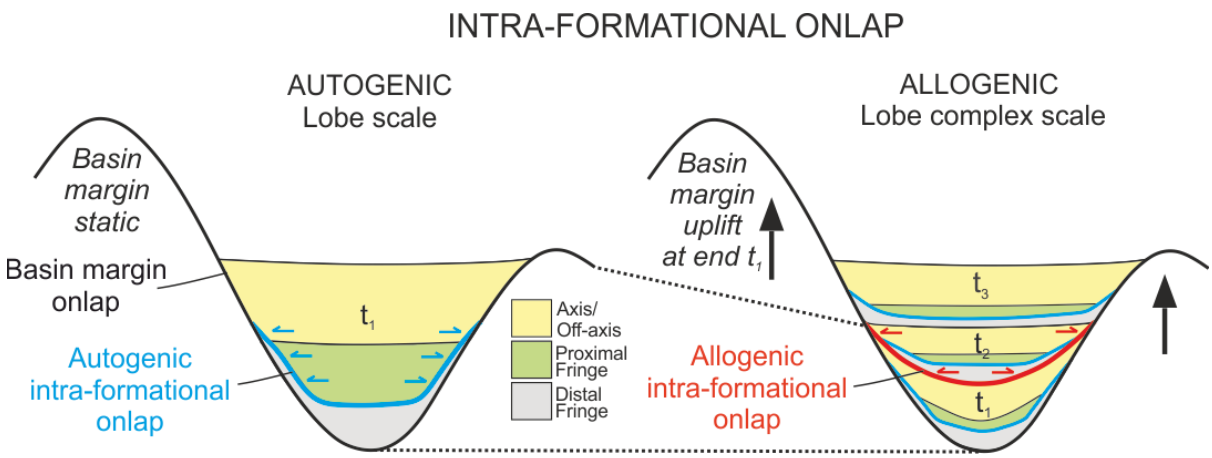

1193
1194

1195

1196

Lithofacies	Description	Interpretation	Facies Association	Onlap Geometry
Thick-bedded sandstone (LF 1)	Forms 1 - 20 m amalgamated packages or 0.5 - 2 m beds, Medium - granule grain size. Flat or erosional bed bases and flat bed tops. Mostly structreless with some planar laminae. Often contains mud clasts (<5 cm) and soft-sediment deformation, e.g. flames and dishes.	Rapid aggradation beneath a highly concentrated flow. Planar-spaced laminae indicate traction-carpet deposition (*sensu* Lowe, 1982).	Lobe axis (FA 1) Lobe off-axis	Abrupt termination High-density flows deposit abruptly at counter-slope due to loss of capacity, compared to lower-concentration flows with otherwise similar flow properties (e.g. Hiscott, 1994). The slope may be draped by deposition from the overriding and dilute tail of the same flow.
Medium-bedded sandstone (LF 2)	0.1 - 0.8 m beds. Fine - coarse grain size. Flat or weakly erosional bed bases and flat or convolute bed tops. Flutes and grooves on bed bases. Sporadic granules sometimes present and associated with structureless lower bed divisions. Mostly normally graded with planar and convolute laminae. Ripples at bed tops.	Presence of flutes, normal grading, and tractional structures indicates deposition from a dilute turbidity current. These beds are interpreted as medium-density turbidites due to their often structureless basal divisions and thicknesses greater than 10 cm.	Lobe off-axis (FA 2) Lobe axis Proximal fringe	Abrupt to draped termination More capable of surmounting topography than higher-density flows because they are more able to maintain turbulent energy while flowing up the counter-slope (e.g., Bakke et al., 2013; Eggenhuisen et al. 2017). Wide variety of sediment concentrations in these flows causes drape to extend from meters to tens of meters up the slope.
Hybrid beds (LF 3)	0.1 - 1.2 m bipartite or tripartite beds. Lower medium-coarse sandstones (division 1) overlain sharply or loaded by argillaceous sandstones (division 2). Argillaceous sandstones often have a sheared fabric. Cleaner, often finer, and tractionally reworked sandstone sometimes present capping these divisions with a sharp or foundered base (division 3). Decimeter scale organic material sometimes present in middle division.	Beds containing deposits of both turbulent and transitional/ laminar flows interpreted as hybrid beds (*sensu* Haughton et al. 2009). Flow transformation occurs through increasing concentration of fines during run-out (e.g., Kane et al. 2017) or through forced deceleration (Barker et al. 2008; Patacci et al. 2014).	Proximal fringe (FA 3) Lobe off-axis Distal fringe Lobe axis	Abrupt to draped termination Debritic or argillaceous middle divisions are highly concentrated so terminate abruptly. Draping of the middle division may occur if the slope is shallow enough to allow run-up of the debritic middle division. The turbulent lower part of the flow may drape the slope and amalgamate with the overlying sandstone or deposit abruptly if high-density.
Thin-bedded sandstone (LF 4)	0.01 - 0.1 m siltstones and fine sandstones. Parallel and convolute laminae, normal grading. Flutes rarely preserved. Ripples occasionally show opposing paleoflow directions.	Fine grain size, thin event beds, and abundance of tractional structures indicates that these beds were deposited by low-density/concentration turbidity current and are therefore interpreted as low-density turbidites.	Distal fringe (FA 4) Proximal fringe Lobe off-axis	Draped termination Low-concentration flows are less affected by changes in slope angle and are thus able to surmount basin topography and drape topography for substantial distances up the counter-slope (e.g., Muck and Underwood, 1990). Low-density turbidites are therefore able to dominate much of the sediment thickness on the upper parts of the confining slope.

1197